A Scube2-Shh feedback loop links morphogen release to morphogen signaling to enable scale invariant patterning of the ventral neural tube

Authors: Zachary M. Collins[1], Kana Ishimatsu[1], Tony Y.C. Tsai[1], and Sean G. Megason[1,*]

[1] Department of Systems Biology, Harvard Medical School, Boston, MA 02115, USA.

*Author for correspondence (megason@hms.harvard.edu)

Running Title: Scaling of Shh patterning by Scube2

Key words: Scaling, morphogen, patterning, sonic hedgehog, robustness, size

Summary Statement: The Shh morphogen gradient can scale to different size tissues by feedback between Scube2 mediated release of Shh and Shh based inhibition of Scube2 expression

Author contributions

Z.M.C. conducted experiments and data analysis. Z.M.C and S.G.M. conceived the study, designed the experiments, and wrote the paper. K.I and Z.M.C. developed the size reduction technique. T.Y.C.T helped develop the image analysis technique and generated the *tg(shha:memCherry)* reporter line. S.G.M. supervised the overall study.

Abstract

To enable robust patterning, morphogen systems should be resistant to variations in gene expression and tissue size. Here we explore how a Shh morphogen gradient in the ventral neural tube enables proportional patterning in embryos of varying sizes. Using a surgical technique to reduce the size of zebrafish embryos and quantitative confocal microscopy, we find that patterning of neural progenitors remains proportional after size reduction. Intriguingly, a protein necessary for Shh release, Scube2, is expressed far from the source of sonic hedgehog production. *scube2* expression levels control Shh signaling extent during ventral neural patterning and conversely Shh signaling represses the expression of *scube2*, thereby restricting its own signaling. *scube2* is disproportionately downregulated in size-reduced embryos, providing a potential mechanism for size-dependent regulation of Shh. This regulatory feedback is necessary for pattern scaling, as demonstrated by a loss of scaling in *scube2* overexpressing embryos. In a manner akin to the expander-repressor model of morphogen scaling, we conclude that feedback between Shh signaling and *scube2* expression enables proportional patterning in the ventral neural tube by encoding a tissue size dependent morphogen signaling gradient.

Introduction

When Lewis Wolpert first posed the “French Flag Problem”, he was seeking the answer to this fundamental question: What systems enable proportional patterning in embryos independent of embryo size? By the time Wolpert formalized this problem, developmental biologists had long known that embryos scale their patterning programs in response to changes in embryo size (Wolpert, 1969). For example, sea urchin larva pattern normally from a single blastomere up to the four-cell stage and amphibian embryos can survive bisection and pattern proportionally at a reduced size (Driesch, 1892; Morgan, 1895; Spemann, 1938; Cooke, 1981). Significant scaling of pattern formation to tissue availability seems to be a near universal property of developing organisms. Yet, as we pass the 50-year

anniversary of Wolpert's work, how morphogen gradients scale to pattern domains of varied sizes remains unclear in many systems.

Recent theoretical studies have proposed mechanisms that could account for scaling of morphogen-mediated patterning (Ben-Zvi and Barkai, 2010; Umulis and Othmer, 2013). Amongst the most prominent of these is a model termed expander-repressor integral feedback control (Ben-Zvi and Barkai, 2010). In this model, a morphogen represses the expression of another gene, known as the expander, that affects the range of the morphogen itself cell-non-autonomously. In such models, morphogen signaling will expand until it has reached an encoded equilibrium. This equilibrium is controlled by the morphogen's repression of the expander, thus enabling "measurement" of the size of the domain in need of patterning. The first biological example of this mechanism was proposed in Xenopus axial patterning. In this original model, ADMP expands BMP signaling by binding Chordin and inhibiting shuttling of BMP towards the ventral side (Francois et al., 2009). However, more recent experimental work implicated another factor, Sizzled, which may play a central role in scaling in a mathematically equivalent manner (Ben-Zvi et al., 2014; Inomata et al., 2013). Expander-like relationships have also been proposed to regulate scaling of Dpp gradients during wing disc growth and even scaling of synthetic patterns in bacterial colonies (Ben-Zvi et al., 2011; Cao et al., 2016; Hamaratoglu et al., 2011).

Though scaling of early axis patterning following size reduction has been extensively studied, the molecular mechanisms through which tissues and organs subsequently scale their patterning has received less attention (Ben-Zvi et al., 2008; Inomata et al., 2013). Previously, scaling of patterning during organ growth has been considered in the fly wing disc, which grows remarkably in size while maintaining proportion (Averbukh et al., 2014; Ben-Zvi et al., 2011; Hamaratoglu et al., 2011). In vertebrates, the developing neural tube has been a powerful model to study morphogen-mediated patterning (Briscoe and Small, 2015). While neural tube patterning does not expand isometrically over

time with growth, embryos of different species maintain consistent embryonic proportions in the face of significant variation in organ size during initial patterning (Kicheva et al., 2014; Uygur et al., 2016).

The vertebrate ventral neural tube is patterned by the morphogen Sonic Hedgehog (Shh; Marti et al., 1995; Roelink et al., 1995). Shh is produced by the notochord and floorplate and induces ventral cell fates over a long range in a dose-dependent manner (Briscoe et al., 2001; Zeng et al., 2001). Shh ligands themselves are dually lipid-modified and are highly lipophilic (Pepinsky et al., 1998; Porter et al., 1996a; Porter et al., 1996b). While mechanisms of Shh transport have long been disputed, biochemical evidence supports soluble Shh as a primary component of long-range signaling, and release of Shh ligands from cell membranes is critical for gradient formation (Burke et al., 1999; Chen et al., 2004; Zeng et al., 2001). Shh release was largely thought to be achieved by the protein Dispatched, but recent work has identified Scube2 as a more potent factor in promoting Shh release (Burke et al., 1999; Creanga et al., 2012; Kawakami et al., 2002; Tukachinsky et al., 2012).

Scube2 is a Signal sequence containing protein with a CUB domain and EGF-like repeats. The role of Scube2 in Shh signaling was first identified from work using the zebrafish *you* mutant which corresponds to *scube2* (Hollway et al., 2006; Kawakami et al., 2005; van Eeden et al., 1996; Woods and Talbot, 2005; Yang et al., 2002). Interestingly, while *scube2* mutants have defects in ventral patterning, *scube2* is predominantly expressed in the dorsal and intermediate neural tube in both mice and zebrafish (Grimmond et al., 2001; Kawakami et al., 2005; Woods and Talbot, 2005). Additionally, epistasis experiments indicated that Scube2 acts upstream of Patched to stimulate Shh signaling (Woods and Talbot, 2005). This effect was also found to be cell-non-autonomous, as mosaic injection of *scube2* mRNA was capable of rescuing Shh-signaling defects over a long range (Hollway et al., 2006; Woods and Talbot, 2005). Studies in cell culture then demonstrated that Scube2 releases Shh from secreting cells cell-non-autonomously (Creanga et al., 2012; Tukachinsky et al., 2012). Recent work concluded that Scube2 may be responsible for catalyzing the shedding of lipids from the Shh ligands, but this model is disputed by previous findings that released Shh remains dually lipid-modified

(Creanga et al., 2012; Jakobs et al., 2014; Jakobs et al., 2016; Tukachinsky et al., 2012). Scube2's cell non-autonomous role in Shh release and unexpected expression pattern led us to wonder whether Scube2 may regulate pattern scaling by acting as an expander, as has recently been hypothesized elsewhere (Shilo and Barkai, 2017). In this work, we use quantitative imaging of cell fate specification in zebrafish to investigate the scaling of ventral neural patterning and the regulatory role of Scube2.

Results

Ventral neural patterning scales with embryo size

Studying mechanisms of scaling during growth or between species of different sizes is difficult because many properties of the patterning system depend on stage or species-specific variables. To study scaling of pattern formation in embryos with comparable genetic backgrounds at matched time points, we developed a technique to reduce the size of zebrafish embryos inspired by classical work in amphibians, as we recently described (Ishimatsu et al., 2018; Morgan, 1895; Spemann, 1938). Two lateral cuts are made across the blastula stage embryo: one to remove cells near the animal pole, to avoid damaging signaling centers crucial to early D-V patterning, and a second to remove yolk near the vegetal pole. (Fig. 1A). With this technique, a significant fraction of embryos pattern normally and develop at a reduced size (Fig. 1B-C).

We measured scaling of neural patterning in size-reduced embryos using quantitative imaging (Megason SG, 2009; Xiong et al., 2013). High-resolution image-stacks of 18-24 hours postfertilization (hpf) stage matched zebrafish embryos were collected under identical settings, during the same imaging session, from matched Anterior-Posterior positions in control and experimentally perturbed embryos (Fig. 1D-E). Imaging volumes were analyzed with custom built software to manually demarcate the dorsoventral axis and width of the neural tube along the length of the dataset (Fig. 1F, Fig. S1). Image intensity values were extracted in a set number of bins along the D-V axis for the left and right halves of the neural tube to normalize for variability in neural tube height. This system allowed

for the quantitative and unbiased comparison of 3-4 somite lengths of neural imaging data from multiple embryos.

Using this imaging platform, we compared the expression of *patched2*—a direct transcriptional target of Shh—with the *tg(ptch2:kaede)* reporter in wild type and size-reduced embryos (Fig. 1G-J) (Huang et al., 2012) . When quantified relative to their respective neural tube dorsal-ventral heights, *tg(ptch2:kaede)* response gradients maintained nearly identical intensity distributions despite neural tube height being 15.0% (+/- 2.8%) smaller in size-reduced embryos in this dataset (N=5), indicating that Shh responses scale following size reduction (Fig. 1I-J). When viewed on an absolute scale, control and size-reduced embryos show clear shifts in the response gradient as measured by the position at which 50% of mean control maximum intensity is reached (p=0.0076) (Fig. 1J). To quantify this effect at the level of cell fate specification, we utilized a triple transgenic imaging strategy based on reporter lines marking *nkx2.2a* (p3 progenitors), *olig2* (pMN and some p3 progenitors), and *dbx1b* (p0, d6 progenitors) (Fig. 1K-L) (Gribble et al., 2007; Jessen et al., 1998; Kinkhabwala et al., 2011; Kucenas et al., 2008). Anterior-posterior averaged intensity profiles were then segmented to form cell fate profiles (see methods and Fig. S2). Using this method, we generated cell fate profiles which can be compared between embryos (Fig. S2). After normalizing for their altered D-V height (which was reduced in this population by 12.2% +/- 2.4% compared to controls), the average of these cell fate profiles of size-reduced embryos were virtually indistinguishable from those of full sized embryos (Fig. 1M). Furthermore, differences between progenitor domain boundary positions were visible when size normalization was removed (Fig. 1N). Statistically significant shifts in the positions of the p2 and pMN upper boundaries were observed only when compared in their absolute coordinates (Fig. 1N). This further demonstrates that ventral neural patterning adjusts to changes in total D-V height.

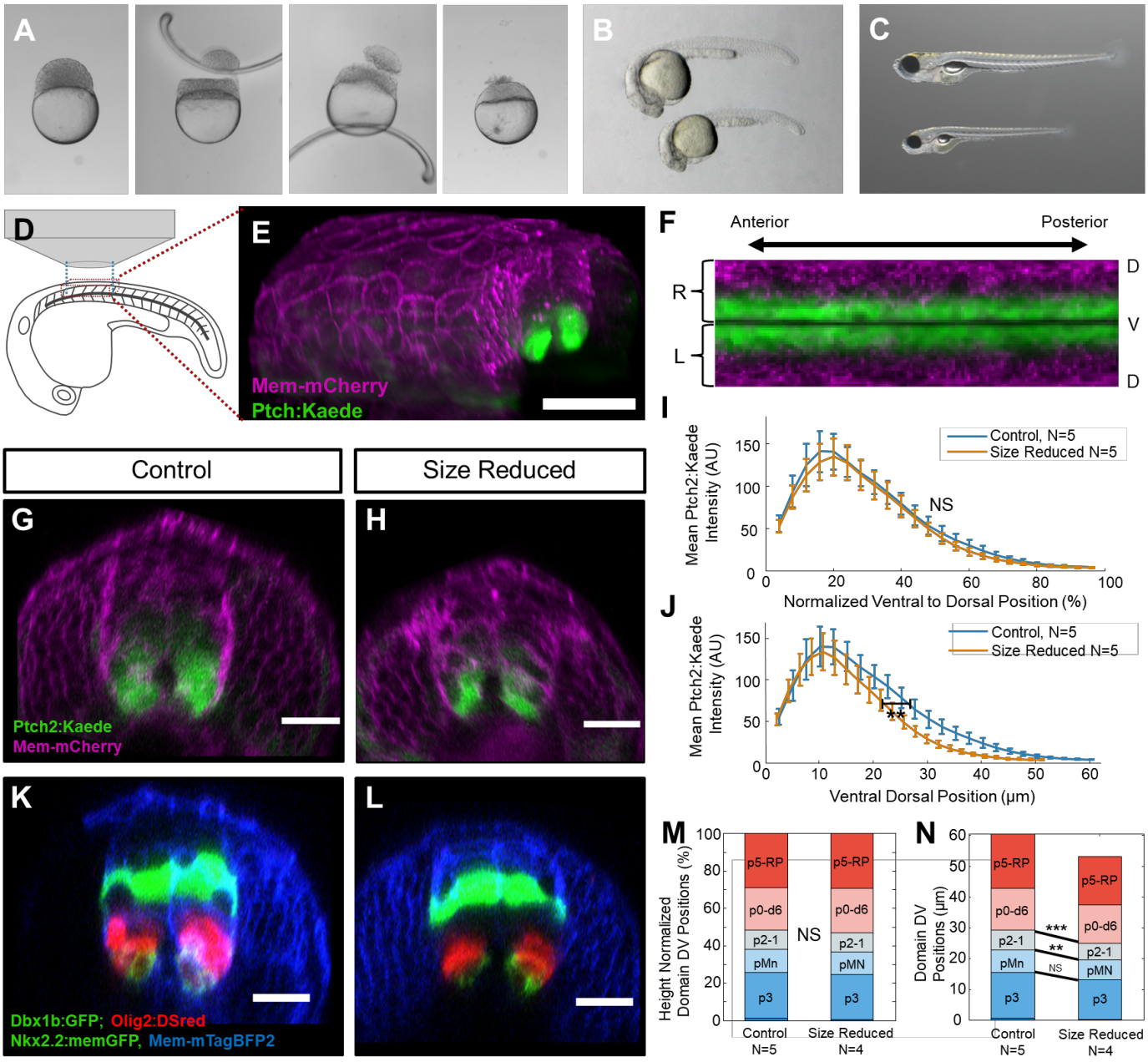

Figure 1- Neural tube patterning scales following embryonic size reduction.

(A) Surgical size reduction of 128-256 cell stage embryos in which cells and yolk are removed to produce smaller embryos (images adapted from Ishimatsu et al. 2018). (B) Example of a size-reduced embryo at 24 hpf (lower) with a normal-sized sibling (upper). (C) Example of a size-reduced larva at six days post fertilization (lower) with a normal-sized sibling (upper). (D) Schematic of an embryo mounted

for imaging; anterior-posterior length of the imaging window is shown with blue lines. Red lines indicate the 3-D extent of the imaging window. (E) 3-D rendering of a confocal z-stack on an example *tg(ptch2:kaede) mem-mCherry* mRNA injected image volume. Scale bar represents 100 µm. (F) Flattened "fillet" profile of segmented imaging data from a z-stack imaged as in E (See methods). (G,H,K,L) Scale bar represents 20 µm. (G-H) Transverse view of 20 hpf *tg(ptch2:kaede)*, *mem-mCherry* mRNA injected control (G) and size-reduced embryos (H). Size reduction led to a decrease in DV height of 15.0% +/- 2.8% in this dataset. (I-J) *ptch2:kaede* intensity profiles from segmented imaging data of embryos from G-H plotted either normalizing for D-V neural tube height (I) or relative to their absolute neural tube heights (J). Error bars indicate standard deviation. No significant shift is observed in the position of 50% mean maximum control intensity on a relative scale between control and size-reduced embryos(I) (unpaired t-test p=0.5981) while a very statistically significant shift in the position is observed when comparing absolute positional values (J) (unpaired t-test p=0.0076; Control N=5, Size Reduced N=5). (K-L) Transverse views of *mem-mtagBFP2* mRNA injected 24 hpf *tg(nkx2:mGFP; olig2:dsred; dbx1b:GFP*) control (K) and size-reduced (L) embryos. Size reduced embryos had an average 12.2% +/- 2.4% reduction in neural tube DV height relative to control embryos in this dataset. (M-N) Results of progenitor domain segmentation analysis (See methods) of embryos treated as in K-L plotted either normalizing for differences in neural tube height (relative scale) (M) or with respect to their endogenous heights (absolute scale) (N). Only when compared on an absolute scale are statistically significant shifts seen in the dorsal boundaries of the p1-p2 and pMN domains (absolute heights unpaired t-test p^{p2}=1.0172e-4 and p^{pMN} =0.0016, Control N=5, Size Reduced N=4). Thresholds for P value significance asterisks: Extremely significant: (< 0.0001) = ****, (0.0001 to 0.001) = ***; Very significant: (0.001 to 0.01) = **; Significant: (0.01 to 0.05) = *.

Scube2 levels control Shh signaling

Based on its role in the cell-non-autonomous regulation of Shh release and its dorsal expression pattern, we hypothesized a potential role for Scube2 in enabling scaling of Shh gradients. This hypothesis depends on *scube2* expression levels having a dose dependent effect on Shh signaling. However, previous work concluded that Scube2 is only required for Shh signaling as a permissive factor (Kawakami et al., 2005; Woods and Talbot, 2005). To examine the role of Scube2 in ventral neural patterning, we performed a morpholino knockdown of *scube2* in *tg(ptch2:kaede*) reporter embryos using a previously validated translation inhibiting morpholino (Fig. 2A-C) (Woods and Talbot, 2005). We observed a decrease in Shh signaling following morpholino injection, as demonstrated by a statistically significant suppression of maximum *ptch2:kaede* intensity (Fig. 2C)(Woods and Talbot, 2005)(Woods and Talbot, 2005)(Woods and Talbot, 2005)(Woods and Talbot, 2005)(Woods and Talbot, 2005). Additionally, quantification of *nkx2.2a, olig2*, and *dbx1b* domain sizes in embryos injected with *scube2* morpholino showed a contraction of ventral progenitor domains (Fig. 2D-F). Ventral shifts in the upper boundaries of the pMN and p3 domains were statistically significant, due in part to near complete elimination of the *nkx2.2a+* p3 domain (Fig. 2F). Unexpectedly, expansion of the p1-2 domain dorsally was also observed, potentially implying long range Shh signaling is required for complete p1-2 induction.

Previous work concluded that Scube2 was a permissive factor based on a lack of ectopic expression of downstream Shh signaling markers as observed by whole mount *in situ* hybridization experiments (Woods and Talbot, 2005). However, our high-resolution quantitative imaging reveals that injection of *scube2* mRNA leads to the expansion of Shh signaling, as shown by broader distributions of *tg(ptch2:kaede*) fluorescence (Fig. 2G-I). Embryos injected with *scube2* mRNA showed significant dorsal shifts in the position of half control maximum *tg(ptch2:kaede*) intensities (p=0.0047), a measure of absolute Shh signaling range (Fig. 2H). Maximum *tg(ptch2:kaede*) fluorescence in *scube2* overexpressing embryos was somewhat higher on average, but not statistically significant (p=0.0512),

194 which may suggest the stronger effect of *scube2* overexpression is to extend the range of Shh
195 signaling. In addition, *scube2* overexpression affected cell type patterning in the ventral neural tube, as
196 measured in triple transgenic *nkx2.2a, olig2,* and *dbx1b* reporter embryos (Fig. 2J-L). Quantification of
197 these cell fate profiles revealed large increases in p3 and pMN domain sizes, a decrease in the size of
198 the p2-p1 domains, and unchanged patterning of the p0-d6 domains and more dorsal cell types.
199 Ventralization was measured by comparing dorsal boundaries of the p3 and pMN, which were
200 statistically significantly shifted (Fig. 2L). These data indicate that not only is Scube2 required for long
201 range Shh signaling, but that *scube2* overexpression amplifies endogenous Shh signaling. Additionally,
202 this suggests that Scube2-stimulated Shh release is a limiting factor in normal patterning.
203

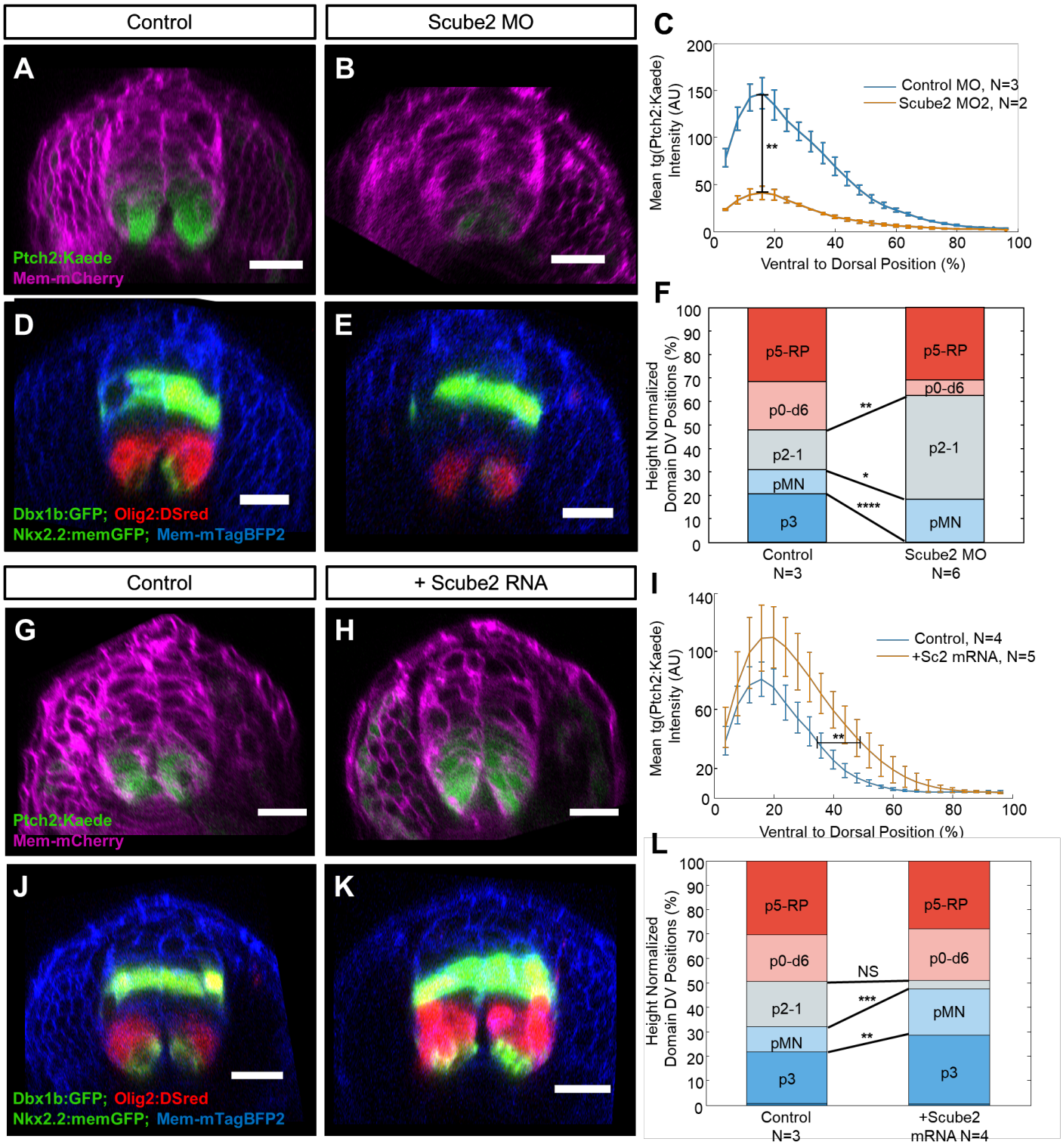

Figure 2- Scube2 expression levels regulate Shh signaling in the ventral neural tube.

(A-B,D-E, G-H, J-K) Transverse view of a confocal z-stack, scale bar represents 20 μm (A-B) Representative image of 22 hpf *tg(ptch2:kaede*) reporter line embryos injected with (A) *mem-mCherry* mRNA with a control morpholino or (B) injected with *mem-mCherry* mRNA and *scube2* morpholino. (C) Quantification of mean intensity distributions in segmented neural tissue from z-stacks of embryos as treated in A-B. Maximum intensities of morpholino treated embryos were very statistically significantly reduced compared to controls (p= 0.0040). (D-E) Representative image of 20 hpf *tg(dbx1b:GFP, olig2:dsred, nkx2.2a:memGFP*) reporter line embryos injected with (D) mem-*mTagBFP2* mRNA alone or (E) co-injected with *scube2* morpholino. (F) Mean result of automated segmentation of progenitor domain sizes (see methods for details) for embryos treated as in D-E. Statistical comparisons of progenitor domain boundaries are shown with connected lines and significance is marked by asterisks. p1-2 domain upper boundaries were shifted dorsally following morpholino treatment ($p^{p1\text{-}2}$= 0.0019), while the upper boundary of pMN and p3 domains were both significantly contracted in morpholino injected embryos (p^{pMN}= 0.0158 and p^{p3}= 9.87e-9). (G-H) Representative image of 20 hpf *tg(*ptch2:kaede) reporter line embryos injected with (G) *mem-mcardinal* mRNA alone or (H) co-injected with *scube2* mRNA. (I) Quantification of mean intensity distributions of embryos as treated in G-H. Dorsoventral position at which half of average control maximum intensity was reached was very significantly shifted in Scube2 overexpressing embryos (unpaired t-test p=0.00470). (J-K) Representative image of 20 hpf *tg(dbx1b:GFP, olig2:dsred, nkx2.2:mGFP*) reporter line embryos injected with (J) *mem-mTagBFP2* mRNA alone or (K) co-injected with *scube2* mRNA. (L) Mean results of automated progenitor domain segmentation of J-K. Statistical comparisons of progenitor domain boundaries are shown with connected lines and significance marked by number of asterisks. pMN and p3 domains were drastically shifted dorsally in *scube2* mRNA injected embryos (p^{MN}=8.6748e-04, and p^{p3}=0.0034 respectively).

Shh negatively regulates Scube2 expression over a long-range

To study Scube2's expression, we developed the *tg(scube2:moxNG*) reporter line containing 7.6KB of the endogenous regulatory sequences driving the extremely bright moxNeonGreen fluorescent protein (Fig. 3A) (Costantini et al., 2015). The expression of *tg*(*scube2:moxNG*) we observed is consistent with previously reported *in situ* hybridizations (Grimmond et al., 2001; Kawakami et al., 2005; Woods and Talbot, 2005). *Tg(scube2:moxNG*) embryos showed very low expression close to the sources of Shh in the floor plate and notochord—as visualized with a transgenic *shh:memCherry* reporter line—and high levels of expression in the dorsal-intermediate neural tube (Fig. 3A-C). Time lapse imaging of *tg(scube2:moxNG*) embryos revealed weak mesodermal expression in the early embryo, which faded during the onset of neurulation and was replaced by high levels of expression in the dorsal and intermediate neural tube (Fig. 3D-G, Movie S1-2).

To test whether Scube2 is downregulated by Shh signaling, we injected mRNA encoding a potent activator of Shh signaling, dnPKA, at the single cell stage and observed the resulting embryos (Hammerschmidt et al., 1996). Embryos injected with *dnpka* mRNA showed near complete ablation of neural *tg(scube2:moxNG*) expression (Fig. 4 A-C). To test whether Shha ligands themselves were capable of suppressing Scube2 expression at a distance, we mosaically overexpressed *shha* in *tg(scube2:moxNG*) embryos by injecting a single blastomere at the 16-cell stage with either *mem-mTagBFP2* alone or with *shha* mRNA (Fig. 4 D-F). We expected local inhibition of Scube2 reporter activity near secreting cells within a few cell diameters. Surprisingly, *tg(scube2:moxNG*) expression was nearly completely eliminated in these embryos indicating potent cell-non-autonomous repression of Scube2 by Shh. When quantified, these embryos demonstrate a highly significant reduction of peak *tg(scube2:moxNG)* intensities (Fig. 4F). To test whether Shh's inhibition of Scube2 is required for its endogenous low ventral expression, we treated embryos with sonidegib, a potent Smoothened antagonist starting at the dome stage. Resulting embryos showed expanded *scube2* expression towards the floor plate and notochord (Fig. 4G-I). Shifts in ventral boundaries were quantified by

254 measuring the D-V position at which 50% of the maximum intensity of the control population was
255 reached. These measurements were statistically significantly shifted in sonidegib-treated embryos
256 relative to controls, indicating that endogenous Shh signaling is responsible for a lack of ventral *scube2*
257 expression (Fig. 4I). A ventral expansion *tg(scube2:moxNG)* was also observed following Cyclopamine
258 treatment, which is consistent with the previous findings of a genomewide screen for genes regulated
259 by Shh signaling (Fig. S3) (Xu et al., 2006). To further probe the transcriptional regulation of Scube2's
260 expression we performed a small scale CRISPR mutagenesis screen and found that Pax6a/b are
261 necessary for driving Scube2 expression. Coinjection of pax6a and pax6b sgRNAs with Cas9 caused
262 significant downregulation of *tg(scube2:moxNG)* relative to control embryos injected with a sgRNA
263 targeting *tyrosinase,* an unrelated pigment gene (Fig. S4).
264

Figure 3- Scube2 is expressed distantly from Shh secreting cells.

(A) Schematic of the *scube2:moxNG* transgenic expression reporter construct used to generate the *tg(scube2:moxNG)* line. (B) Wide-field fluorescence image of *tg(scube2:moxNG)* embryo at 20 hpf. (C) Transverse view of *mem-mTagBFP2*-injected *tg(scube2:moxNG; shh:mem-mCherry)* embryo at 20 hpf. Scale bar represents 20 µm. (D-G) Transverse view from a time-lapse imaging dataset of *tg(scube2:moxNG; shh:memCherry)* embryo which was injected at the single cell stage with *mem-mTagBFP2* mRNA. Time in hours post fertilization is displayed in the bottom right corner. Scale bar represents 50 µm. (D) At early neurulation stages there is weak mesodermal expression of *scube2:moxNG* in the notochord. In addition, expression of *scube2:moxNG* is visible in neural progenitors as the neural plate converges. (E) By 12.5 hpf a pronounced gap in expression of neural progenitors between *shh:mem-mCherry* and *scube2:moxNG* cells is visible. (F) Expansion of the scube2+ domain dorsally is visible as cells continue to converge. (G) *scube2* expression is constricted to the dorsal-intermediate neural tube.

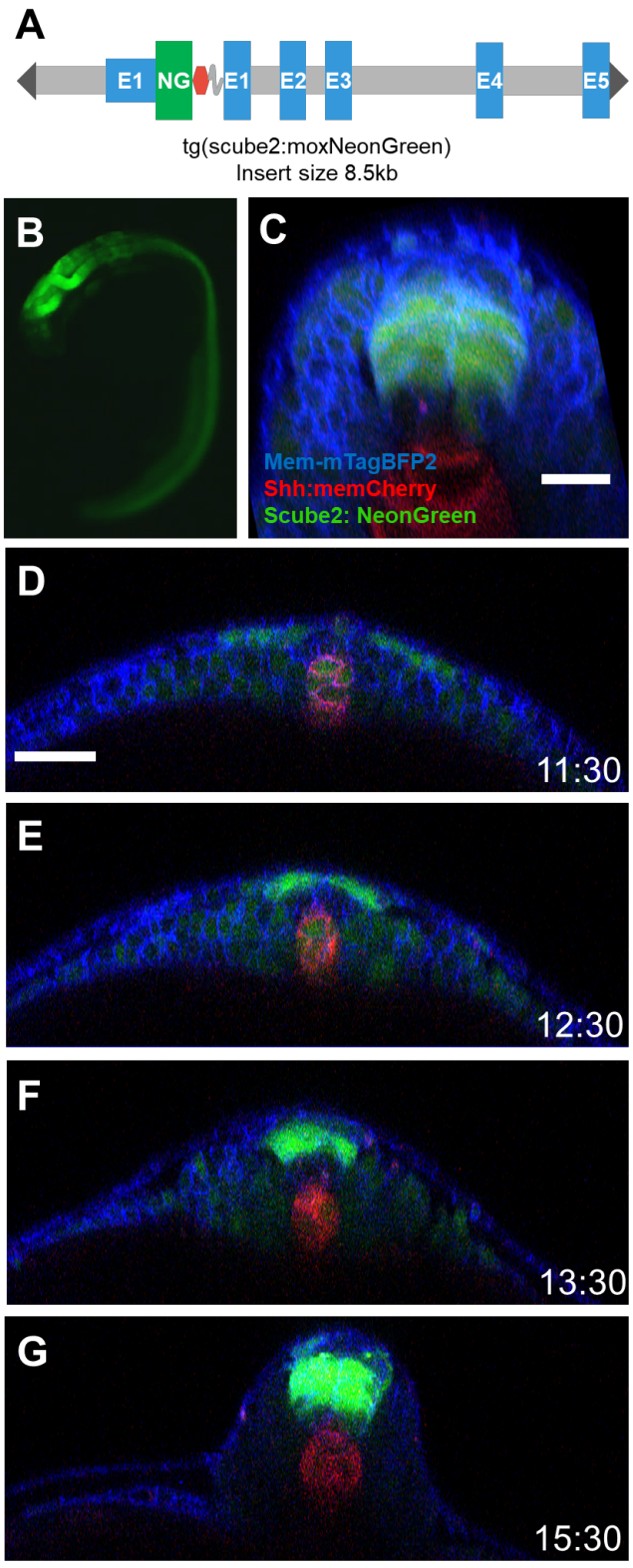

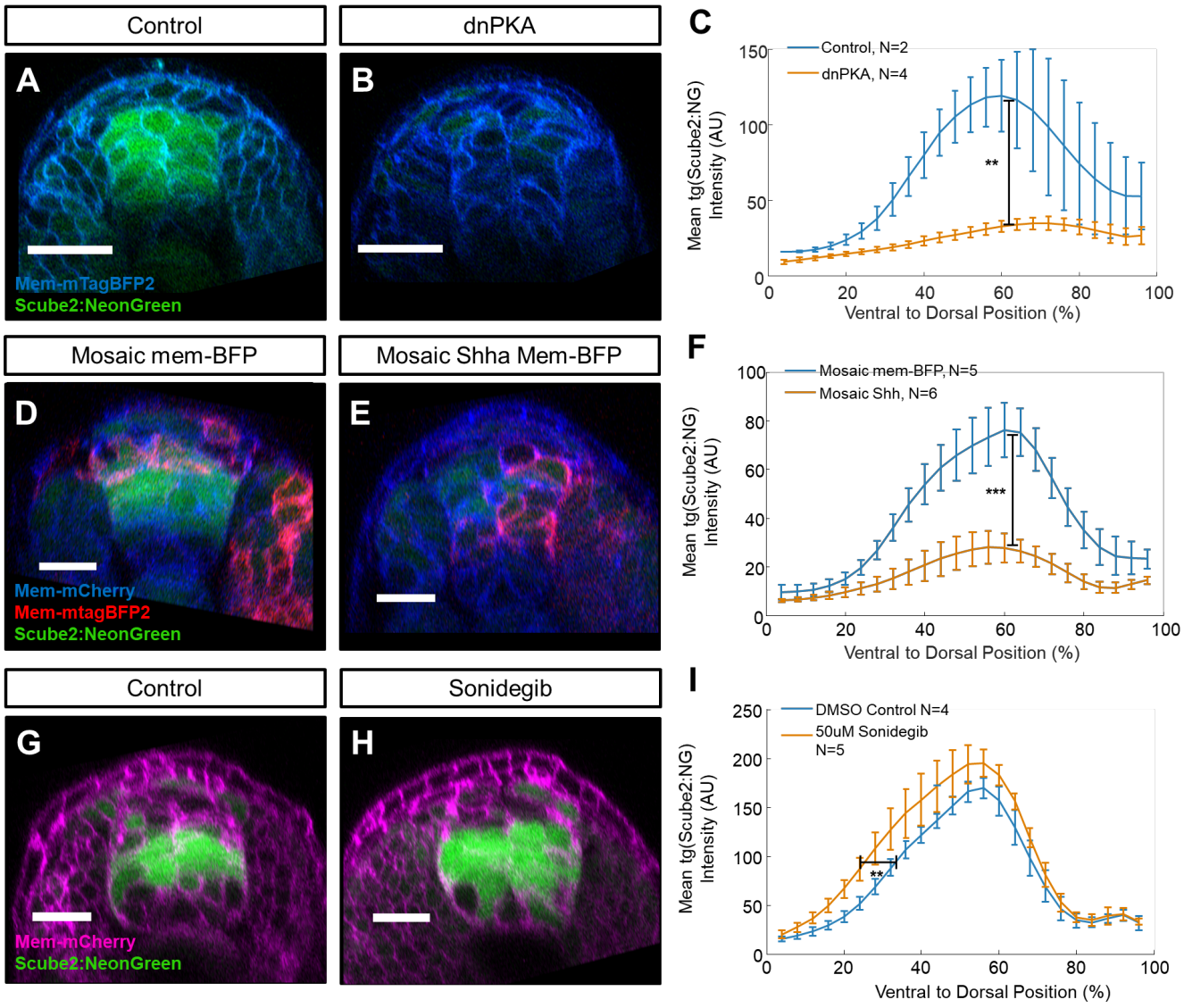

290

291 **Figure- 4 Shh signaling represses Scube2 expression.**

292 (A-B, D-E, G-H) Scale bar represents 20 µm (A-B) Transverse view of 18 hpf *tg(scube2:moxNG)*

293 reporter line embryos injected with (A) *mem-mTagBFP2* mRNA alone or (B) co-injected with *dnpka*

294 mRNA. (C) Quantification of mean reporter intensity of embryos as treated in A-B. Maximum

295 *scube2:moxNG* intensity values were very significantly reduced in *dnpka* mRNA-injected embryos (p=

296 0.0014). (D-E) Transverse view 20 hpf *tg(scube2:moxNG)* reporter line embryos injected at the single

297 cell stage with *mem-mCherry* mRNA and then injected in one blastomere at the 8-16 cell stage with

298 either (D) *mem-mTagBFP2* mRNA alone or (E) co-injected with *shha* mRNA. (F) Quantification of mean
299 reporter intensity of embryos as treated in D-E. Maximum *scube2:moxNG* reporter intensity is extremely
300 significantly reduced in *shha* injected embryos (p= 9.14e-06). (G-H) Transverse view 22 hpf
301 *tg(scube2:moxNG*; *mem:mCherry)* embryos treated with a DMSO control (G) or treated with 50 µm
302 Sonidegib (H). (I) Quantification of mean reporter intensity of embryos as treated in G-H. The black
303 bracket marks the position of 50% of control maximum intensity used for statistical testing. These
304 values were very significantly shifted ventrally in drug treated embryos relative to control (unpaired t-
305 test p=0.0014.).
306

Scube2 diffuses over long distances during patterning

While Scube2 is known to act cell non-autonomously from transplantation experiments and Scube2-conditioned media has a potent Shh release stimulating effect *in vitro*, the localization of Scube2 protein during development is unknown (Woods and Talbot, 2005; Creanga et al., 2012). *In vitro*, Scube2 is thought to associate with Heparin Sulfate Proteoglycans, and Scube2 had been hypothesized to diffuse from secreting cells in the dorsal neural tube, the need for which was later disputed (Jakobs et al., 2016; Kawakami et al., 2005; Hollway et al., 2006). To examine Scube2's localization, we developed Scube2 fluorescent fusion proteins by tagging the C-terminus as previously validated in cell culture with other tags (Fig. 5A) (Creanga et al., 2012). The resulting Scube2-mCitrine fusion proteins were functional and rescued Scube2 CRISPR mutants at comparable rates to wildtype Scube2 (Fig. S5). Mosaic injection of *scube2-mCitrine* mRNA at the 32-64 cell stage revealed that Scube2-mCitrine diffuses distantly from producing cells (Fig. 5B). Following single cell mRNA injection, Scube2-mCitrine fusions were secreted and did not remain associated with cell membranes, as demonstrated by their presence in the extracellular space between cells marked with mem-mCherry (Fig. 4C).

To assay Scube2's rate of diffusion we performed Fluorescence Recovery After Photobleaching (FRAP) at the dome stage, during which cell movement is minimal. FRAP was performed in a 100µm x 100µm region and recovery was observed at 10 second intervals over 5 minutes (Fig. 5 D-E, Movie S3-4). Image data from the bleached region was then normalized to its initial intensity and fitted to recovery curves using standard methods (Munjal et al., 2015). We find that the addition of Scube2 to mCitrine causes only minor changes to its diffusion (Fig. 5F-G). No significant differences were observed between the calculated mobile fractions of Scube2-mCitrine (0.283 +/- 0.018) and Sec-mCitrine (0.338+/- 0.019; unpaired t-test p=0.0698). When the time to 50% recovery of the mobile fraction is calculated, Scube2-mCitrine has modestly slower diffusion time than Sec-mCitrine alone (Fig. 5 F-G;

p=0.0405). These data further support Scube2's diffusion in the extracellular space, which likely mediates its long range of effect.

To observe distributions of Scube2 during development, we generated a transgenic line expressing the full length Scube2 protein fused to moxNeonGreen under control of Scube2 regulatory sequences (Fig. 5H-K). We validated the functionality of this *Tg(scube2:scube2-moxNG)* line using a morpholino which bound only endogenous Scube2 at the splice junction of exon6, and not *Tg(scube2:scube2-moxNG)* derived RNA which lacks this splice junction (Figure S6). *Tg(scube2:scube2-moxNG)* embryos were markedly resistant to treatment with this morpholino, validating the in vivo functionality of this construct (Figure S6). *Tg(scube2:scube2-moxNG)* embryos showed broad distributions of Scube2 during patterning (Fig. 5H-K). Throughout early patterning Scube2-moxNeonGreen is visible near ventral cells marked by *tg(shha:mem-mCherry*), although Scube2 is expressed largely in the dorsal neurectoderm at this timepoint (Fig. 5H-I, Movie S5-6). By 24 hpf *tg(scube2:scube2-moxNG)* fluorescence is found distributed throughout the embryo, although expression from *tg(scube2:moxNG)* is localized to the dorsal-intermediate neurectoderm. These data further suggest that Scube2's long range of effect can be explained by diffusion from secreting cells in the intermediate and dorsal neural tube to the source of Shh in the floor plate and notochord.

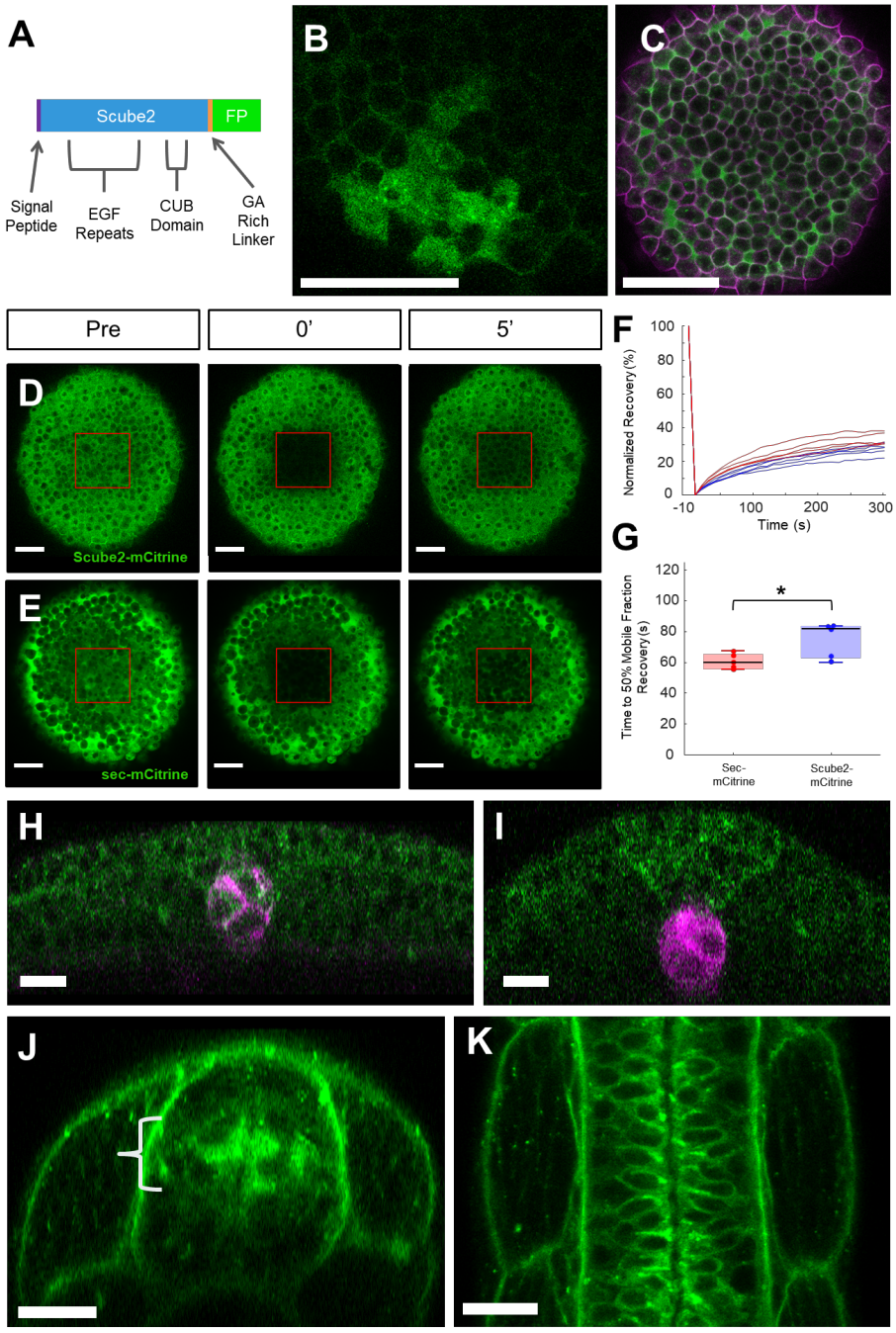

Figure 5- Scube2 diffuses from secreting cells and is broadly distributed during patterning.

(A) Schematic of Scube2-mCitrine fluorescent fusion protein design. (B-C) Scale bar represents 100 µm. (B) Scube2-mCitrine fluorescence at the sphere stage from embryos injected in one blastomere at the 64-cell stage with *scube2-mCitrine* mRNA. Cells from the injected clone are marked by intracellular

(secretory system) fluorescence. (C) Scube2-mCitrine fluorescence from embryos injected at the single cell stage with *scube2-mCitrine* and *membrane mCherry* mRNA. (D-E) Fluorescence recovery after photobleaching at the dome stage of Scube2-mCitrine (D) and Secreted-mCitrine (E). (F) Raw FRAP recovery traces normalized to maximum intensity pre-bleach and minimum intensity following bleaching. Red lines represent Secreted-mCitrine and blue lines represent Scube2-mCitrine. (G) A boxplot comparing the time at which 50% recovery of mobile fraction is achieved from dome stage FRAP data. Bracket with asterisk denotes unpaired t-test comparison between Scube2-mCitrine and Sec-mCitrine ($p = .0405$) (H-K) Scale bar represents 20 μm. (H) Transverse view of an 11.5 hpf *tg(sc2:sc2-moxNG;shh:mem-mCherry)* embryo. (I) Transverse view of a 14 hpf *tg(sc2:sc2-moxNG; shh:mem-mCherry)* embryo. (G) Transverse view of a 24 hpf *tg(scube2:scube2-moxNG)* embryo. (K) Horizontal view of the embryo from J.

365 **Feedback regulation of Scube2 levels is necessary for pattern scaling**

366 To examine the regulation of Scube2 in size-reduced embryos, we performed our size reduction
367 technique on *tg(scube2:moxNG; shha:mem-mCherry)* embryos and imaged them at 20 hours post
368 fertilization. Unlike other observed patterning genes, *scube2* expression levels did not scale in size-
369 reduced embryos but were instead severely reduced (Fig. 6A-C). This finding is consistent with an
370 expander-repressor-like model of Scube2-Shh. In this regime, inhibition of *scube2* expression in size-
371 reduced embryos would contract Shh signaling, enabling adjustment of Shh signaling for a decreased
372 tissue size (Fig. 6D-E).

373 Next, we examined whether feedback control of *scube2* expression levels by Shh signaling is
374 required for pattern scaling by saturating *scube2* levels by over-expression. If Scube2 is responsible for
375 adjusting Shh signaling during scaling, we would expect *scube2*-overexpressing size-reduced embryos
376 to have the same absolute Shh response profiles as controls, which would fail to scale following size
377 normalization (Fig. 6F-G). If scaling of ventral patterning is not dependent on Scube2, we would expect
378 maintenance of pattern scaling with size-proportionate increases in *ptch2:kaede* distributions in both
379 populations. We overexpressed *scube2* by mRNA injection in *ptch2:kaede* reporter embryos. When
380 normalized for differences in D-V heights, size-reduced *scube2*-overexpressing embryos showed a
381 disproportionate expansion of the Ptch signaling gradient compared to normal-sized *scube2*-
382 overexpressing embryos (Fig. 6H-K). Dorsal expansion of Shh signaling is quantified using the position
383 of 50% of average maximum control intensity, which is statistically significantly shifted dorsally in size-
384 reduced embryos (Fig. 6J). Importantly, when *tg(ptch2:kaede)* response profiles are plotted on an
385 absolute rather than relative scale, they nearly exactly overlap (Fig. 6K). This overlap without size
386 normalization suggests that *scube2* overexpression encodes a response profile which is independent of
387 embryo size and is not secondarily tuned by another scaling related factor. This strongly suggests that
388 control of *scube2* expression levels is required for scaling the Shh response gradient.

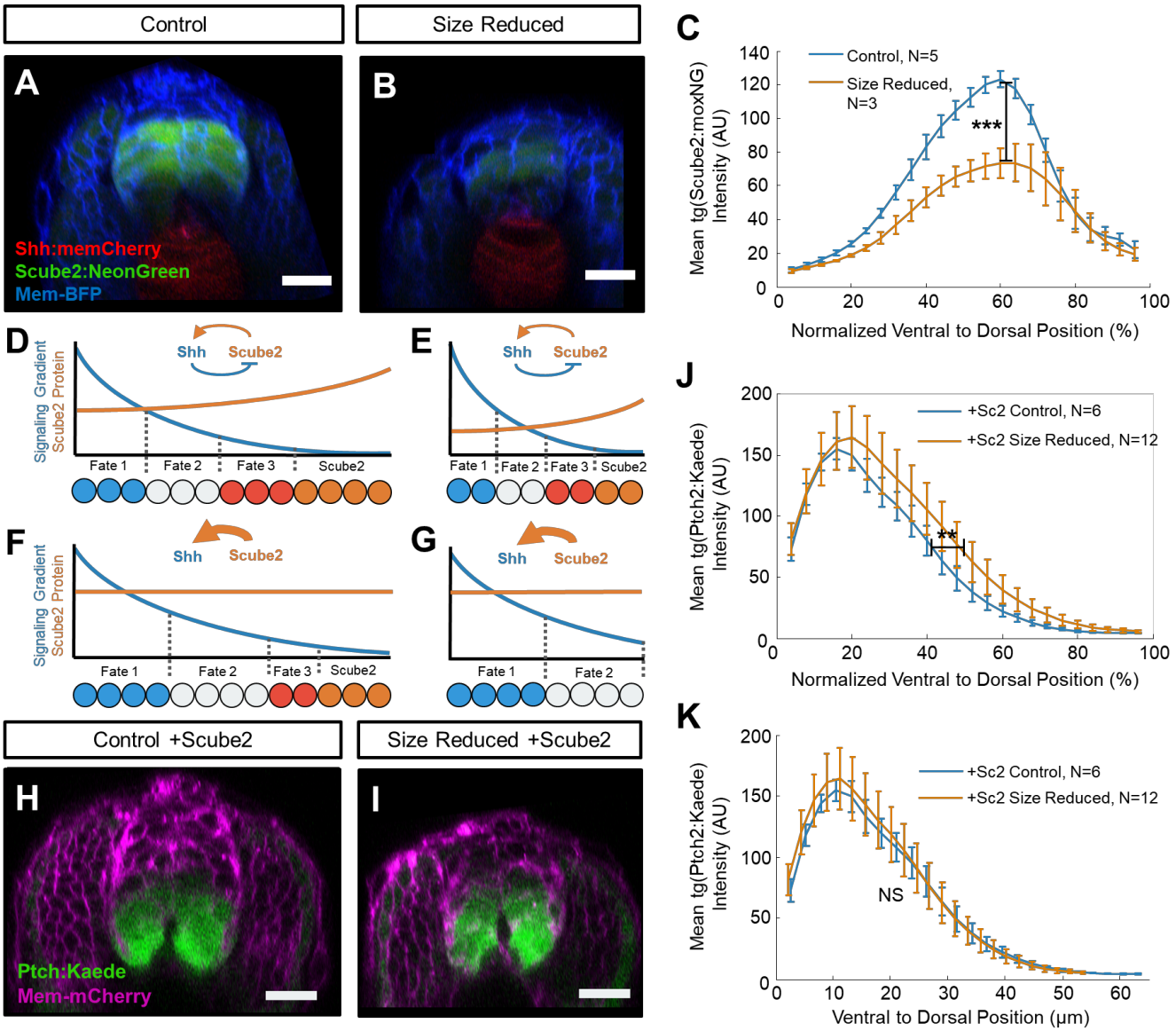

Figure 6- Scube2 expression is size-dependent and required for pattern scaling.

(A-B) Transverse view of *mem-mTagBFP2* mRNA-injected *tg(scube2:moxNG; shh:mem-mCherry)* control (A) or size-reduced (height reduction of 17.1% +/- 7.7%) (B) embryos at 20 hpf. (C) Quantification of mean *tg(scube2:moxNG)* intensity versus ventral-to-dorsal position of embryos from A-B. Maximum intensity values are statistically significantly reduced in treated embryos (p=3.03e-4). (D-E) Schematic of expander-repressor-like feedback control of Shh signaling by Scube2 and its ability to enable pattern scaling. Repression of Scube2 by Shh encodes an equilibrium level of Shh signaling

397 across the tissue by linking morphogen spread to tissue size. (F-G) Schematic representation of the
398 experiment as performed in H-K, where Scube2 levels are at saturation due to overexpression, and
399 size-reduced embryos (G) are disproportionately affected. (H-I) Transverse view of 20 hpf
400 *tg(ptch2:kaede)* control (H) and size-reduced (I) embryos injected with *mem-mCherry* and *scube2*
401 mRNA. (J) Quantification of mean *tg(ptch2:kaede)* intensity versus normalized ventral-to-dorsal position
402 of embryos treated as in H-I. Very significant shifts are observed in the dorsal position of 50% of the
403 maximum intensity value (unpaired t-test p=0.0092). (K) Intensity profiles from J rescaled to reflect the
404 absolute scale of the measurements (DV height reduction of 15.2% +/- 2.1%). When measured in these
405 coordinates, no difference is observed in the position of half of maximum intensity (p= 0.9760).

406

Discussion

Our work uncovers that the morphogen Sonic Hedgehog can self-regulate to enable scale-invariant patterning through linking morphogen signaling to inhibition of Scube2. We discovered that patterning of the neural tube adjusts to tissue availability following surgical size reduction in zebrafish embryos. Using overexpression experiments we demonstrate that Scube2's activity during patterning is not just permissive—overexpression of *scube2* quantiatively enhances Shh signaling (Woods and Talbot, 2005). Utilizing a transgenic reporter line which we developed, we characterized the expression of Scube2 during neural patterning and found that Shh signaling is responsible for its repression in the ventral neural tube. Using Scube2 fluorescent fusion proteins we found that Scube2 is broadly distributed from secreting cells, explaining its previously reported cell non-autonomous activity (Creanga et al., 2012; Woods and Talbot, 2005). Unlike other patterning genes, *scube2* responds to changes in neural tube height by disproportionately decreasing its expression, and overexpression of Scube2 inhibits scaling of the Shh signaling gradient by circumventing its feedback control. The expression of *scube2* thus can be seen as comparable to the "size-dependent factor" Sizzled, which is thought to enable scaling in early D-V patterning by tuning its expression levels to embryo size by chordin-dependent feedback inhibition (Inomata et al., 2013).

The relationship between Scube2 and Shh has important similarities to proposed "expander-repressor" models of morphogen scaling (Barkai and Ben-Zvi, 2009; Ben-Zvi and Barkai, 2010; Inomata et al., 2013). As with expanders in these models, *scube2* enhances morphogen range, is repressed by morphogen signaling, and acts cell non-autonomously at a distance from its source. However, Scube2's reported role in morphogen release may be distinct from the proposed mechanism of expanders. Expanders extend the range of morphogens by promoting their diffusion or inhibiting their degradation (Ben-Zvi and Barkai, 2010). While release of Shh ligands from secreting cells would support their transport, the potentially irreversible nature of this effect and local action at the morphogen source would make distinct predictions for Scube2's effects on morphogen distributions. Nonetheless our study

marks the first observation of an expander-repressor-like relationship outside of the BMP/Dpp signaling pathway in a developing organism. This finding raises the possibility that expander-repressor-like relationships may be common motifs in the regulation of morphogen gradients.

We began this work in part due to interest in the discrepancy between the area of Scube2's activity in the ventral neural tube and its expression in the dorsal neural tube. Our work with Scube2 fluorescent protein fusions revealed that Scube2 is diffusive and is distributed broadly from producing cells. Scube2's diffusion from producing cells could easily account for the distance between its expression domain and area of effect (Figure 5). Scube2's broad distribution and considerable extracellular diffusivity bolsters the hypothesis that Scube2 may serve as a chaperone for Shh during its transport as hypothesized previously (Tukachinsky et al., 2012). Cell culture experiments have indicated that Scube2 cooperates with Dispatched in a cholesterol-dependent "hand off" by binding different domains on Shh's cholesterol moiety (Tukachinsky et al., 2012). Continued binding of Scube2 to the hydrophobic sterol domain may facilitate the un-hindered diffusion of Shh through the extracellular millieu. This model is consistent with the dose dependency we observe in our Scube2 overexpression experiments (Figure 2G-L) and may help solve the puzzle of the long-range transport of dually lipid modified hedgehog in vertebrates. Further investigation of the strength and duration of Scube2 and Shh's binding in vivo may shed light on this relationship. Unfortunately, direct imaging of this phenomenon is hampered by the lack of fully functional Shh fluorescent protein fusions (Chamberlain et al., 2008).

While some evidence suggests that Scube2 plays a role in lipid-shedding, these observations conflict with previous HPLC analysis and the findings of independent groups which demonstrated that Shh species released by Scube2 are dually lipid modified (Creanga et al., 2012; Tukachinsky et al., 2012). If correct, a model of Scube2 in which it acts only transiently at the cell surface of producing cells—either by enabling the formation of multimeric Shh complexes or lipid shedding—would have interesting implications for its role as an expander. Expanders are often formalized as having a dose

457 dependent reversible effect on morphogen spread, while a transient role of Scube2 in Shh multimeric
458 complex formation or shedding would be localized and irreversible. Mathematical modeling may reveal
459 interesting implications of each proposed mechanism in Scube2-Shh feedback interactions during
460 pattern scaling.

461 Scube2 is one of several recently identified elements of the Shh signaling pathway that exerts
462 cell non-autonomous effects. Recent work has shown that Hhip—initially characterized as a membrane-
463 tethered hedgehog antagonist—acts over a long range that cannot be explained by ligand
464 sequestration (Kwong et al., 2014). Additionally, the Hedgehog receptor, Patched, may also have cell
465 non-autonomous inhibitory effects on Smoothened through regulating inhibitory sterols or sterol
466 availability (Bidet et al., 2011; Roberts et al., 2016). Together with known feedback relationships and
467 the diffusivity of Scube2 that we demonstrated here, these mechanisms interlink Shh signaling between
468 neighboring cells and may enable tissue level properties, such as the scaling of pattern formation we
469 observed.

470 However, scaling of neural patterning is unlikely to be achieved by regulation of Shh signaling
471 alone. BMP signaling in the dorsal neural tube is known to pattern dorsal progenitors. Scaling of BMP
472 signaling in dorsal neural patterning may be achieved via a similar or carry-over mechanism to early D-
473 V axis patterning and should be explored in further studies. In the early D-V patterning system, both
474 existing models propose expander-like relationships between elements of the BMP signaling pathway.
475 The first model proposed ADMP as a scaling related factor, while more recent research has
476 demonstrated that Sizzled has an indispensable role in scaling (Ben-Zvi et al., 2008; Ben-Zvi et al.,
477 2014; Inomata et al., 2013). During neural patterning, the BMP antagonists Noggin, Follistatin, and
478 Chordin are expressed in the notochord while BMP ligands are expressed in the roof plate. Intriguingly,
479 while Sizzled does not seem to be expressed during neural patterning, ADMP is expressed in the
480 notochord and thus may play a role in the scaling of BMP-mediated patterning of the dorsal neural tube
481 (Willot et al., 2002).

BMP signaling is known to increase the thresholds for Shh-dependent cell fate specification, making signaling integration between these pathways a potential additional candidate regulator of scaling (Liem et al., 2000; McHale et al., 2006). Inhibition of either Shh or BMP signaling causes expansion of signaling by the alternative program. In normal patterning, cells do not measure ratios of BMP and Shh. In fact, Dbx1 positive progenitors in the medial neural tube require little to no Shh or BMP signaling present in order to be specified (Pierani et al., 1999). In addition, recent experiments with precise control of Shh and BMP concentrations in an explant system have shown that cells choose either ventral or dorsal fates in the presence of significant BMP and Shh signaling (Zagorski et al., 2017). Regulation of *scube2* expression may be another way to enable crosstalk between signaling pathways, as *scube2* is not expressed in the dorsal most cells of the spinal cord, suggesting repression by dorsal factors. Specification of the dorsal boundary of *scube2* expression may encode yet more information about the size of the tissue which would then affect Shh spread.

Methods

Generation of Transgenic Lines

The construct used to make *tg(scube2:moxNG)* was generated by isothermal assembly of PCR-amplified *scube2* regulatory elements obtained from the CHORI-211 BAC library. Regulatory elements were in part chosen based on annotations of H3K4me1 and H3K4me3 binding (Aday et al., 2011). Selected regulatory sequences spanned 1677bp of upstream intergenic sequence and 5962bp of the area spanning exons 1-5 *scube2*. Regulatory sequences were cloned into a pMT backbone by placing a zebrafish codon-optimized moxNeonGreen fluorescent protein and sv40 poly-A tail just downstream of the endogenous *scube2* Kozak sequence (Costantini et al., 2015). The construct used to make *tg(scube2:scube2-moxNG)* was generated using the same regulatory sequences as

506 *tg(scube2:moxNG*), with the addition of cDNA corresponding to exons 6-23 of the Scube2 coding
507 sequence downstream of exon 5 and moxNeonGreen attached at the c-terminus with a 10 amino acid
508 long GA rich linker. The construct used to make *tg(shh:mem-mCherry)* was derived from the previously
509 reported *tg(shh:GFP*), by replacement of GFP with mem-mCherry (Megason, 2009; Shkumatava et al.,
510 2004).

511 Transgenic lines were generated by injecting plasmid DNA for each construct along with Tol2
512 mRNA into wild type (AB) embryos at the single cell stage, as described previously (Kawakami, 2004).
513 moxNeonGreen positive embryos were then selected for raising. Upon reaching sexual maturity, F0s
514 were outcrossed and screened for founders. Founders were isolated and raised as single alleles.
515 Monoallelic versions of each line are shown throughout the paper.

516 **Zebrafish Strains**

517 For wild type lines, AB fish were used. All fish were kept at 28°C on a 14-hour-light/10-hour-dark
518 cycle. Embryos were collected from natural crosses. All fish-related procedures were carried out with
519 the approval of Institutional Animal Care and Use Committee (IACUC) at Harvard University.
520 tgBAC(*ptch2:kaede*) (Huang et al., 2012; renamed from *ptch1* due to a change in zebrafish gene
521 nomenclature), *tg(nkx2.2a:mGFP)* (Jessen et al., 1998), *tg(olig2:GFP)* (Shin et al., 2003),
522 *tg(olig2:dsRed)* (Kucenas et al., 2008), and tgBAC(*dbx1b:GFP)* (Kinkhabwala et al., 2011) have been
523 described previously.

524 **Size Reduction Technique.**

525 Size reduction was performed as described in our previous report (Ishimatsu et al., 2018). Embryo
526 sizes were reduced by sequentially removing ~1/3 of the cells from the animal cap, then wounding the
527 yolk. These surgeries are performed in 1/3 ringers solution, and embryos are immobilized in a thin layer
528 of 2% methyl cellulose. Surgeries can be performed either with glass needles – as previously described

529 – or using a loop of thin stainless-steel wire that is inserted through a glass capillary tube and mounted
530 on a halved chopstick as done here. Healthy uninjected embryos show a maximum success rate of
531 ~60% while embryos which have undergone injection or were spawned by older females have
532 significantly lower success rates. In each size reduction experiment, embryos are screened for health
533 and the largest size reductions; those with insufficient size reduction or morphological defects are
534 discarded.

535 **Construct Generation and Injections of mRNAs and Morpholinos**

536 Scube2-mCitrine was generated from cDNA obtained from the Talbot lab (Woods and Talbot, 2005).
537 Fluorescent protein fusions were made by attaching mCitrine or moxNeonGreen with a 10 amino acid
538 GA rich linker to the c-terminus of Scube2. Membrane-mTagBFP2 constructs were generated using
539 membrane localization tags reported previously (Megason, 2009; Subach et al., 2011). These
540 constructs were each sub-cloned into a pMTB backbone. mRNA for all experiments was synthesized
541 from pCS or pMTB backbones via *in vitro* transcription using the mMESSAGE mMACHINE system
542 (Ambion). Embryos were injected at the single cell stage using a Nanoject system set to 2.3nl of
543 injection volume containing 70-90pg of RNA for each mRNA injected. Injected embryos were then
544 screened for brightness, and damaged embryos were removed. Scube2 morpholino injections were
545 performed with 7ng of Scube2 MO2 and 3.5ng of p53 MO to control for phenotypic variability, while
546 control morpholino injections were performed using 10.5ng of p53 MO only (Gerety and Wilkinson,
547 2011; Woods and Talbot, 2005).

548 **Sonidegib and Cyclopamine Treatment**

549 Stock solution of 1 mM Sonidegib suspended in DMSO was used for treatment as generously given by
550 the lab of Rosalind Segal. Embryos were placed in egg water containing a concentration of 50µM for
551 the treatment condition, and equal parts DMSO were added to the sham control. Cyclopamine was

552 dissolved in 100% ethanol to make 50mM stock solution and was diluted for treatment in egg water to
553 100 µM. Treatment began at 7 hpf and continued until imaging at 22 hpf.

554 **Confocal Imaging**

555 For quantitative imaging, embryos were staged and mounted in our previously described dorsal mount
556 (Kimmel et al., 1995; Megason, 2009; Xiong et al., 2013) in egg water with 0.01% tricaine (Western
557 Chemical, Inc.). Embryos were manipulated for proper positioning with hair loops, before gently
558 lowering the coverslip. Embryos were not depressed by the coverslip or impinged by the mold, enabling
559 imaging of their normal proportions. Imaging was performed on embryos staged at 18-24 hpf, unless
560 otherwise noted in corresponding figure legends. Live imaging was performed using a Zeiss 710
561 confocal/2-photon microscope, Zen image acquisition software, and C-Apochromat 40X 1.2 NA
562 objective. For fluorescent protein excitation, 405 nm (BFP), 488 nm (GFP/moxNeonGreen), 514 nm
563 (mCitrine), 561 nm (mCherry/dsRed) and 594 nm (mCardinal) lasers were used. The imaging field was
564 centered in each embryo on the somite 6/7 boundary for consistent positioning between images. For
565 quantitative analysis, imaging datasets are only compared between sibling embryos imaged on the
566 same day with the same settings. This approach aims to avoid clutch effects or variability in detector
567 sensitivity and laser power that occur over time. Typical imaging settings with the 40x objective were as
568 follows: image size of 1024x1024 pixels with .21µm per pixel and an interval of 1µm in the Z direction.
569 For display purposes, images are rendered in cross sectional views (X-Z axis) which are then rotated
570 for display, with image intensities for co-injection markers adjusted evenly within datasets for
571 displayable brightness. FRAP, early stage embryo imaging and time-lapses were performed using a 1.0
572 NA 20x objective. Brightfield and widefield fluorescence images of whole embryos were obtained using
573 an Olympus MVX10 and a Leica MZ12.5 dissecting microscope.
574

575 **FRAP Experiments and Analysis**

Imaging for FRAP was performed using a 1.0 NA 20x objective at dome stage. Bleaching was performed for two minutes in a 100µmx100µm area in the center of the frame with a 488nm Argon laser. Imaging was performed with a low laser power to reduce bleaching, and images were obtained at 10 second intervals over five minutes to quantify recovery. FRAP data in the bleached region was then normalized to the minimum and maximum intensity for each respective time trace. Normalized recovery intensities were then fitted to the following exponential to determine the mobile fraction (*A*) in MATLAB: $y = A(1 - e^{-\tau t})$ (Munjal et al., 2015). These fitted traces were also used to determine the point at which 50% maximum recovery was reached in Figure 5G.

Image Analysis

Images were analyzed using a custom MATLAB-based image analysis software that enables rapid segmentation of neural tube imaging data. Neural imaging data is segmented by the user sequentially from anterior to posterior. Over a set step size (usually 50 pixels), the user selects points at the base of the floor plate cell and top of the roof plate cell that divide the neural tube into its two halves (Fig. S1A). The user then selects the widest point of the neural tube in each image. Imaging data from mature neurons, found laterally, and within the lumen of the neural tube, found medially, are disregarded using a set percentage of neural width (Fig. S1B). Once these positions are recorded, imaging data is then recovered as average pixel intensity in 25 bins from ventral to dorsal across 3-4 somites of A-P length. This binning and averaging strategy enables comparison of data between embryos that accounts for variations in neural tube D-V height. During the segmentation process, the researcher is blinded to the title of the dataset which contains information about its treatment condition. For distribution plots, binned intensities are reported for each embryo as the average intensities for each bin along the entire AP axis of the imaging volume. Each embryo's average intensity profile is then treated as an independent sample and averaged for displayed distribution profiles and standard deviations. To avoid

artifacts caused by rounding in the calculations of half maximum control intensity positional values are extracted from the spline-interpolated intensity profiles for each individual dataset.

Progenitor domain segmentation is performed on average intensity profiles from each embryo in a dataset in the following manner: first, all intensity profiles in the data set undergo background subtraction and cross channel fluorescence caused by the extreme brightness of the *dbx1b:GFP* line is removed from the *olig2:dsred* channel. Intensity profiles are then fed to a peak finding algorithm to identify local maxima. Both *dbx1b+* and *nkx2.2a+* progenitor domains are found in the green channel, so a maximum of two peaks is allowed. In the red channel, only one peak is specified to identify *olig2:dsred* signal. Average peak intensity values for each domain are then calculated for the entire control dataset, and 50% of this value in the case of the *nkx2.2a* and *dbx1b* domains is used as the threshold for calculating domain width. Given its greater spread along the D-V axis, a threshold of 25% of peak height is used in calculating width of the *olig2+* domain. Domain widths are then extracted from spline-interpolated intensity profiles to avoid errors introduced by rounding to the next bin. Segmented widths and positions of *nkx2.2a*, *olig2*, and *dbx1b* expression are then averaged for plotting purposes. Domain plots are generated by assigning all *nkx2.2a*+ progenitors to the p3 fate, *olig2*+ progenitors lacking *nkx2.2a* expression overlap to the pMN fate, and *dbx1b*+ progenitors to the p0-d6 fate. These domain sizes and positions are then used to reconstruct domains in-between or flanking them, which include the p2-p1 domain between pMN and p0-d6, the floorplate below p3, and the d5-roofplate above p0-d6. These heights and positions are then used to generate the stacked bar plots shown.

Statistical Analysis

Statistical comparisons of maximum average intensity and position of 50% maximum intensity are performed by an unpaired T-test. Although each dataset contains hundreds of measurements of each binned intensity value over the A-P axis of a z-stack, only the average of these measurements for each embryo is treated as a data-point for calculation of the standard deviation and statistical

significance tests. This is done to avoid oversampling that would exaggerate statistical significance. In all measurements, statistical significance is markedly increased if analysis is performed by treating all underlying intensity measurements as samples. Thresholds for calculating the position of half maximum are determined from the average maximum of the corresponding control dataset for each experiment. Position is then determined from the fitted trend-line to avoid inaccuracies due to rounding. To calculate the significance of shifts in boundary positions, upper domain boundaries for each embryo were compared in an un-paired t-test between embryos from each population. When the progenitor domain segmentation algorithm finds there is no domain present, the boundary is set to 0.

CRISPR Screen for Scube2 Regulators

Cas9 protein was generated and purified in lab as described (Gagnon et al., 2014). Three guide RNA sequences targeting the first one-to-three exons of each gene were selected based on their quality using the web-tool CHOP-CHOP and synthesized using standard methods (Gagnon et al., 2014). Equivalent guide RNA and Cas9 protein concentrations were used in all samples for mosaic knockout. Phenotypes were assessed at 18-20 hpf by confocal microscopy.

Acknowledgments

We thank Lisa Goodrich, Rosalind Segal, and Wolfram Goessling for their comments and helpful discussion. The Scube2 construct was a gift from the Talbot lab.

Competing interest

The authors declare no competing or financial interests.

Funding

Z.M.C was supported in part by the program in Biological and Biomedical Sciences at Harvard University. S.G.M. and Z.M.C. were supported by R01-GM107733 and R01-DC015478. T.Y.-C.T. was supported by the Damon Runyon Cancer Foundation Fellowship.

References

Aday, A. W., Zhu, L. J., Lakshmanan, A., Wang, J. and Lawson, N. D. (2011). Identification of cis regulatory features in the embryonic zebrafish genome through large-scale profiling of H3K4me1 and H3K4me3 binding sites. *Dev. Biol.* **357**, 450–462.

Averbukh I, Ben-Zvi D, Mishra S, Barkai N, Averbukh, I., Ben-Zvi, D., Mishra, S. and Barkai, N. (2014). Scaling morphogen gradients during tissue growth by a cell division rule. *Development* **141**, 2150–6.

Barkai, N. and Ben-Zvi, D. (2009). "Big frog, small frog"--maintaining proportions in embryonic development: delivered on 2 July 2008 at the 33rd FEBS Congress in Athens, Greece. *FEBS J.* **276**, 1196–207.

Ben-Zvi, D. and Barkai, N. (2010). Scaling of morphogen gradients by an expansion-repression integral feedback control. *Proc. Natl. Acad. Sci. U. S. A.* **107**, 6924–9.

Ben-Zvi, D., Shilo, B.-Z., Fainsod, A. and Barkai, N. (2008). Scaling of the BMP activation gradient in Xenopus embryos. *Nature* **453**, 1205–11.

Ben-Zvi, D., Pyrowolakis, G., Barkai, N. and Shilo, B.-Z. (2011). Expansion-repression mechanism for scaling the Dpp activation gradient in Drosophila wing imaginal discs. *Curr. Biol.* **21**, 1391–6.

Ben-Zvi, D., Fainsod, A., Shilo, B.-Z. and Barkai, N. (2014). Scaling of dorsal-ventral patterning in the Xenopus laevis embryo. *Bioessays* **36**, 151–6.

Bidet, M., Joubert, O., Lacombe, B., Ciantar, M., Nehmé, R., Mollat, P., Brétillon, L., Faure, H., Bittman, R., Ruat, M., et al. (2011). The Hedgehog Receptor Patched Is Involved in Cholesterol Transport. *PLoS One* **6**, e23834.

Briscoe, J. and Small, S. (2015). Morphogen rules: design principles of gradient-mediated embryo patterning. *Development* **142**, 3996–4009.

Briscoe, J., Chen, Y., Jessell, T. M. and Struhl, G. (2001). A hedgehog-insensitive form of patched provides evidence for direct long-range morphogen activity of sonic hedgehog in the neural tube. *Mol. Cell* **7**, 1279–91.

Burke, R., Nellen, D., Bellotto, M., Hafen, E., Senti, K.-A. A., Dickson, B. J. and Basler, K. (1999). Dispatched, a Novel Sterol-Sensing Domain Protein Dedicated to the Release of Cholesterol-Modified Hedgehog from Signaling Cells. *Cell* **99**, 803–815.

Cao, Y., Ryser, M. D., Payne, S., Li, B., Rao, C. V. and You, L. (2016). Collective Space-Sensing Coordinates Pattern Scaling in Engineered Bacteria. *Cell* **165**, 620–630.

Chamberlain, C. E., Jeong, J., Guo, C., Allen, B. L. and McMahon, A. P. (2008). Notochord-derived Shh concentrates in close association with the apically positioned basal body in neural target cells and forms a dynamic gradient during neural patterning. *Development* **135**, 1097–106.

Chen, M.-H., Li, Y.-J., Kawakami, T., Xu, S.-M. and Chuang, P.-T. (2004). Palmitoylation is required for the production of a soluble multimeric Hedgehog protein complex and long-range signaling in vertebrates. *Genes Dev.* **18**, 641–59.

Cooke, J. (1981). Scale of body pattern adjusts to available cell number in amphibian embryos. *Nature* **290**, 775–778.

Costantini, L. M., Baloban, M., Markwardt, M. L., Rizzo, M., Guo, F., Verkhusha, V. V. and Snapp, E. L. (2015). A palette of fluorescent proteins optimized for diverse cellular environments. *Nat. Commun.* **6**, 7670.

Creanga, A., Glenn, T. D., Mann, R. K., Saunders, A. M., Talbot, W. S. and Beachy, P. A. (2012). Scube/You activity mediates release of dually lipid-modified Hedgehog signal in soluble form. *Genes Dev.* **26**, 1312–25.

Driesch, H. (1892). Entwicklungsmechanische Studien: I. Der Werthe der beiden ersten Furchungszellen in der Echinogdermenentwicklung. Experimentelle Erzeugung von Theil- und Doppelbildungen. *Zeitschrift für wissenschaftliche Zool.*

Francois, P., Vonica, A., Brivanlou, A. H. and Siggia, E. D. (2009). Scaling of BMP gradients in Xenopus embryos. *Nature* **461**, E1–E1.

Gagnon, J. A., Valen, E., Thyme, S. B., Huang, P., Ahkmetova, L., Pauli, A., Montague, T. G., Zimmerman, S., Richter, C., Schier, A. F., et al. (2014). Efficient Mutagenesis by Cas9 Protein-Mediated Oligonucleotide Insertion and Large-Scale Assessment of Single-Guide RNAs. *PLoS One* **9**, e98186.

Gerety, S. S. and Wilkinson, D. G. (2011). Morpholino artifacts provide pitfalls and reveal a novel role for pro-apoptotic genes in hindbrain boundary development. *Dev. Biol.* **350**, 279–89.

Gribble, S. L., Nikolaus, O. B. and Dorsky, R. I. (2007). Regulation and function of Dbx genes in the zebrafish spinal cord. *Dev. Dyn.* **236**, 3472–83.

Grimmond, S., Larder, R., Van Hateren, N., Siggers, P., Morse, S., Hacker, T., Arkell, R. and Greenfield, A. (2001). Expression of a novel mammalian epidermal growth factor-related gene during mouse neural development. *Mech. Dev.* **102**, 209–211.

Hamaratoglu, F., de Lachapelle, A. M., Pyrowolakis, G., Bergmann, S. and Affolter, M. (2011). Dpp signaling activity requires Pentagone to scale with tissue size in the growing Drosophila wing imaginal disc. *PLoS Biol.* **9**, e1001182.

Hammerschmidt, M., Bitgood, M. J. and McMahon, A. P. (1996). Protein kinase A is a common negative regulator of Hedgehog signaling in the vertebrate embryo. *Genes Dev.* **10**, 647–58.

Hollway, G. E., Maule, J., Gautier, P., Evans, T. M., Keenan, D. G., Lohs, C., Fischer, D., Wicking, C. and Currie, P. D. (2006). Scube2 mediates Hedgehog signalling in the zebrafish embryo. *Dev. Biol.* **294**, 104–18.

Inomata, H., Shibata, T., Haraguchi, T. and Sasai, Y. (2013). Scaling of dorsal-ventral patterning by embryo size-dependent degradation of Spemann's organizer signals. *Cell* **153**, 1296–311.

Ishimatsu, K., Hiscock, T. W., Collins, Z. M., Sari, D. W. K., Lischer, K., Richmond, D. L., Bessho, Y., Matsui, T. and Megason, S. G. (2018). Size-reduced embryos reveal a gradient scaling-based mechanism for zebrafish somite formation. *Development* **145**, dev161257.

Jakobs, P., Exner, S., Schürmann, S., Pickhinke, U., Bandari, S., Ortmann, C., Kupich, S., Schulz, P., Hansen, U., Seidler, D. G., et al. (2014). Scube2 enhances proteolytic Shh processing from the surface of Shh-producing cells. *J. Cell Sci.* **127**, 1726–37.

Jakobs, P., Schulz, P., Ortmann, C., Schürmann, S., Exner, S., Rebollido-Rios, R., Dreier, R., Seidler, D. G. and Grobe, K. (2016). Bridging the gap: heparan sulfate and Scube2 assemble Sonic hedgehog release complexes at the surface of producing cells. *Sci. Rep.* **6**, 26435.

Jessen, J. R., Meng, A., McFarlane, R. J., Paw, B. H., Zon, L. I., Smith, G. R. and Lin, S. (1998). Modification of bacterial artificial chromosomes through Chi-stimulated homologous recombination and its application in zebrafish transgenesis. *Proc. Natl. Acad. Sci.* **95**, 5121–5126.

Kawakami, K. (2004). Transgenesis and Gene Trap Methods in Zebrafish by Using the Tol2 Transposable Element.pp. 201–222.

Kawakami, T., Kawcak, T., Li, Y.-J., Zhang, W., Hu, Y. and Chuang, P.-T. (2002). Mouse dispatched mutants fail to distribute hedgehog proteins and are defective in hedgehog signaling. *Development* **129**, 5753–65.

Kawakami, A., Nojima, Y., Toyoda, A., Takahoko, M., Satoh, M., Tanaka, H., Wada, H., Masai, I., Terasaki, H., Sakaki, Y., et al. (2005). The zebrafish-secreted matrix protein you/scube2 is implicated in long-range regulation of hedgehog signaling. *Curr. Biol.* **15**, 480–8.

Kicheva, A., Bollenbach, T., Ribeiro, A., Valle, H. P., Lovell-Badge, R., Episkopou, V. and Briscoe, J. (2014). Coordination of progenitor specification and growth in mouse and chick spinal cord. *Science (80-.).* **345**, 1254927–1254927.

Kimmel, C. B., Ballard, W. W., Kimmel, S. R., Ullmann, B. and Schilling, T. F. (1995).

751 Stages of embryonic development of the zebrafish. *Dev. Dyn.* **203**, 253–310.

752 **Kinkhabwala, A., Riley, M., Koyama, M., Monen, J., Satou, C., Kimura, Y., Higashijima,**
753 **S.-I. and Fetcho, J.** (2011). A structural and functional ground plan for neurons in the hindbrain
754 of zebrafish. *Proc. Natl. Acad. Sci. U. S. A.* **108**, 1164–9.

755 **Kucenas, S., Takada, N., Park, H.-C., Woodruff, E., Broadie, K. and Appel, B.** (2008).
756 CNS-derived glia ensheath peripheral nerves and mediate motor root development. *Nat. Neurosci.*
757 **11**, 143–151.

758 **Kwong, L., Bijlsma, M. F. and Roelink, H.** (2014). Shh-mediated degradation of Hhip allows cell
759 autonomous and non-cell autonomous Shh signalling. *Nat. Commun.* **5**, 4849.

760 **Liem, K. F., Jessell, T. M. and Briscoe, J.** (2000). Regulation of the neural patterning activity of
761 sonic hedgehog by secreted BMP inhibitors expressed by notochord and somites. *Development*
762 **127**, 4855–4866.

763 **Liu, T.-L., Upadhyayula, S., Milkie, D. E., Singh, V., Wang, K., Swinburne, I. A.,**
764 **Mosaliganti, K. R., Collins, Z. M., Hiscock, T. W., Shea, J., et al.** (2018). Observing
765 the cell in its native state: Imaging subcellular dynamics in multicellular organisms. *Science* **360**,
766 eaaq1392.

767 **McHale, P., Rappel, W.-J. and Levine, H.** (2006). Embryonic pattern scaling achieved by
768 oppositely directed morphogen gradients. *Phys. Biol.* **3**, 107–120.

769 **Megason, S. G.** (2009). In toto imaging of embryogenesis with confocal time-lapse microscopy.
770 *Methods Mol. Biol.* **546**, 317–32.

771 **Morgan, T. H.** (1895). Half embryos and whole embryos from one of the first two blastomeres. *Anat.*
772 *Anz.* **10**, 623–638.

773 **Munjal, A., Philippe, J.-M., Munro, E. and Lecuit, T.** (2015). A self-organized biomechanical
774 network drives shape changes during tissue morphogenesis. *Nature* **524**, 351–355.

775 **Pepinsky, R. B., Zeng, C., Wen, D., Rayhorn, P., Baker, D. P., Williams, K. P., Bixler,**
776 **S. A., Ambrose, C. M., Garber, E. A., Miatkowski, K., et al.** (1998). Identification of a
777 Palmitic Acid-modified Form of Human Sonic hedgehog. *J. Biol. Chem.* **273**, 14037–14045.

778 **Pierani, A., Brenner-Morton, S., Chiang, C. and Jessell, T. M.** (1999). A sonic hedgehog-
779 independent, retinoid-activated pathway of neurogenesis in the ventral spinal cord. *Cell* **97**, 903–
780 15.

781 **Porter, J. A., Ekker, S. C., Park, W.-J., von Kessler, D. P., Young, K. E., Chen, C.-H.,**
782 **Ma, Y., Woods, A. S., Cotter, R. J., Koonin, E. V, et al.** (1996a). Hedgehog Patterning

Activity: Role of a Lipophilic Modification Mediated by the Carboxy-Terminal Autoprocessing Domain. *Cell* **86**, 21–34.

Porter, J. A., Young, K. E. and Beachy, P. A. (1996b). Cholesterol Modification of Hedgehog Signaling Proteins in Animal Development. *Science (80-.).* **274**, 255–259.

Roberts, B., Casillas, C., Alfaro, A. C., Jägers, C. and Roelink, H. (2016). Patched1 and Patched2 inhibit Smoothened non-cell autonomously. *Elife* **5**,.

Shilo, B.-Z. and Barkai, N. (2017). Buffering Global Variability of Morphogen Gradients. *Dev. Cell* **40**, 429–438.

Shin, J., Park, H.-C., Topczewska, J. M., Mawdsley, D. J. and Appel, B. (2003). Neural cell fate analysis in zebrafish using olig2 BAC transgenics. *Methods Cell Sci.* **25**, 7–14.

Shkumatava, A., Fischer, S., Müller, F., Strahle, U. and Neumann, C. J. (2004). Sonic hedgehog, secreted by amacrine cells, acts as a short-range signal to direct differentiation and lamination in the zebrafish retina. *Development* **131**, 3849–58.

Spemann, H. (1938). *Embryonic Development and Induction*. Yale Univ.; New Haven:

Subach, O. M., Cranfill, P. J., Davidson, M. W. and Verkhusha, V. V. (2011). An Enhanced Monomeric Blue Fluorescent Protein with the High Chemical Stability of the Chromophore. *PLoS One* **6**, e28674.

Tukachinsky, H., Kuzmickas, R. P. P., Jao, C. Y. Y., Liu, J. and Salic, A. (2012). Dispatched and Scube Mediate the Efficient Secretion of the Cholesterol-Modified Hedgehog Ligand. *Cell Rep.* **2**, 308–320.

Umulis, D. M. and Othmer, H. G. (2013). Mechanisms of scaling in pattern formation. *Development* **140**, 4830–43.

Uygur, A., Young, J., Huycke, T. R., Koska, M., Briscoe, J. and Tabin, C. J. (2016). Scaling Pattern to Variations in Size during Development of the Vertebrate Neural Tube. *Dev. Cell* **37**, 127–135.

van Eeden, F. J. J., Granato, M., Schach, U., Brand, M., Furutani-Seiki, M., Haffter, P., Hammerschmidt, M., Heisenberg, C. P. P., Jiang, Y. J. J., Kane, D. A. A., et al. (1996). Mutations affecting somite formation and patterning in the zebrafish, Danio rerio. *Development* **123**, 153–164.

Willot, V., Mathieu, J., Lu, Y., Schmid, B., Sidi, S., Yan, Y.-L., Postlethwait, J. H., Mullins, M., Rosa, F. and Peyriéras, N. (2002). Cooperative Action of ADMP- and BMP-Mediated Pathways in Regulating Cell Fates in the Zebrafish Gastrula. *Dev. Biol.* **241**, 59–78.

Wolpert, L. (1969). Positional information and the spatial pattern of cellular differentiation. *J. Theor. Biol.* **25**, 1–47.

Woods, I. G. and Talbot, W. S. (2005). The you gene encodes an EGF-CUB protein essential for Hedgehog signaling in zebrafish. *PLoS Biol.* **3**, e66.

Xiong, F., Tentner, A. R., Huang, P., Gelas, A., Mosaliganti, K. R., Souhait, L., Rannou, N., Swinburne, I. a, Obholzer, N. D., Cowgill, P. D., et al. (2013). Specified neural progenitors sort to form sharp domains after noisy Shh signaling. *Cell* **153**, 550–61.

Xu, J., Srinivas, B. P., Tay, S. Y., Mak, A., Yu, X., Lee, S. G. P., Yang, H., Govindarajan, K. R., Leong, B., Bourque, G., et al. (2006). Genomewide expression profiling in the zebrafish embryo identifies target genes regulated by Hedgehog signaling during vertebrate development. *Genetics* **174**, 735–52.

Yang, R.-B., Ng, C. K. D., Wasserman, S. M., Colman, S. D., Shenoy, S., Mehraban, F., Komuves, L. G., Tomlinson, J. E. and Topper, J. N. (2002). Identification of a novel family of cell-surface proteins expressed in human vascular endothelium. *J. Biol. Chem.* **277**, 46364–73.

Zagorski, M., Tabata, Y., Brandenberg, N., Lutolf, M. P., Tkačik, G., Bollenbach, T., Briscoe, J. and Kicheva, A. (2017). Decoding of position in the developing neural tube from antiparallel morphogen gradients. *Science* **356**, 1379–1383.

Zeng, X., Goetz, J. A., Suber, L. M., Scott, W. J., Schreiner, C. M. and Robbins, D. J. (2001). A freely diffusible form of Sonic hedgehog mediates long-range signalling. *Nature* **411**, 716–20.

841 **Supplemental Figures:**

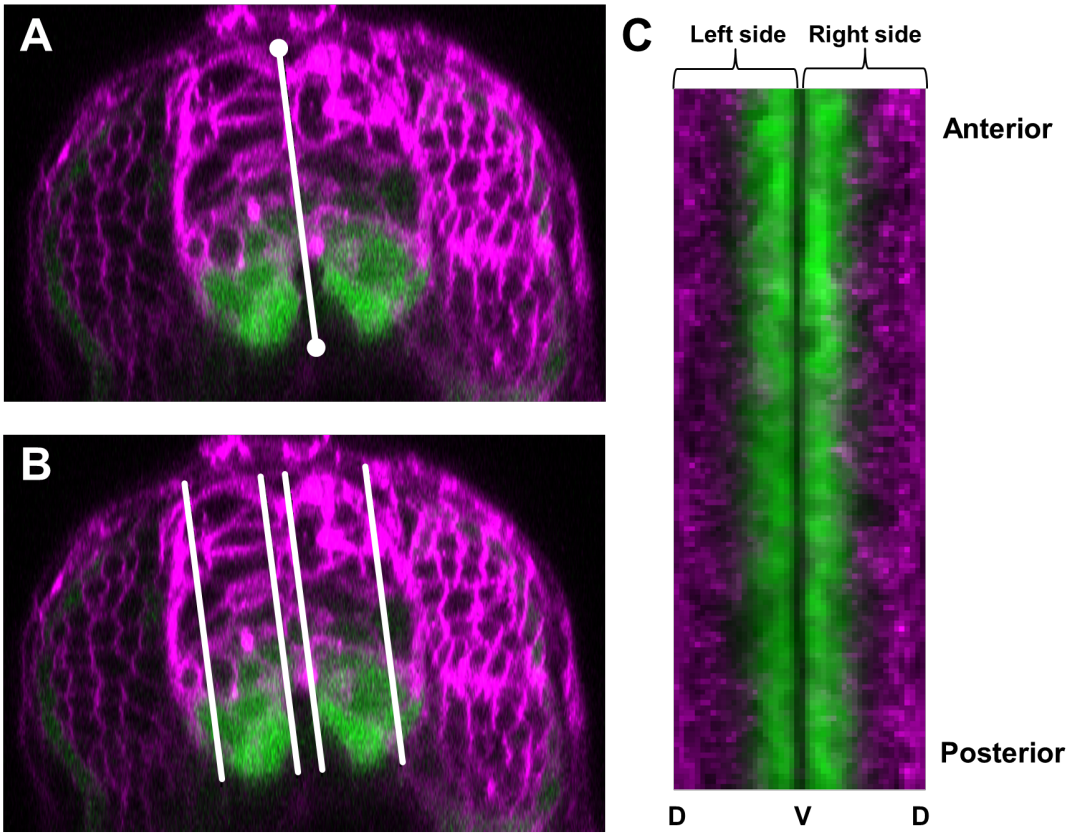

842

843 **Figure S1- Segmentation of neural imaging data.**

844 (A) Image of a 20 hpf *tg(ptch2:kaede)* reporter embryo undergoing selection of the "axis of reflection"
845 which serves to mark a measurement of Dorsoventral height and separate the left and right halves of
846 the neural tube. These positions are picked by the user, first by picking the bottom of the floor plate cell,
847 then inputting the top coordinate of the roof plate cell. (B) Image of a 20 hpf *tg(ptch2:kaede)* reporter
848 embryo after a user has selected the width of the spinal cord. The algorithm then calculates how much
849 imaging data to collect based on a ratio which avoids mature neurons and the lumen of the spinal cord.
850 (C) After collection of average intensities in each bin, data is stored as shown. Average profiles for
851 generating distribution plots and segmenting domains are gathered by averaging these data along the
852 A-P axis for both halves of the neural tube.

853

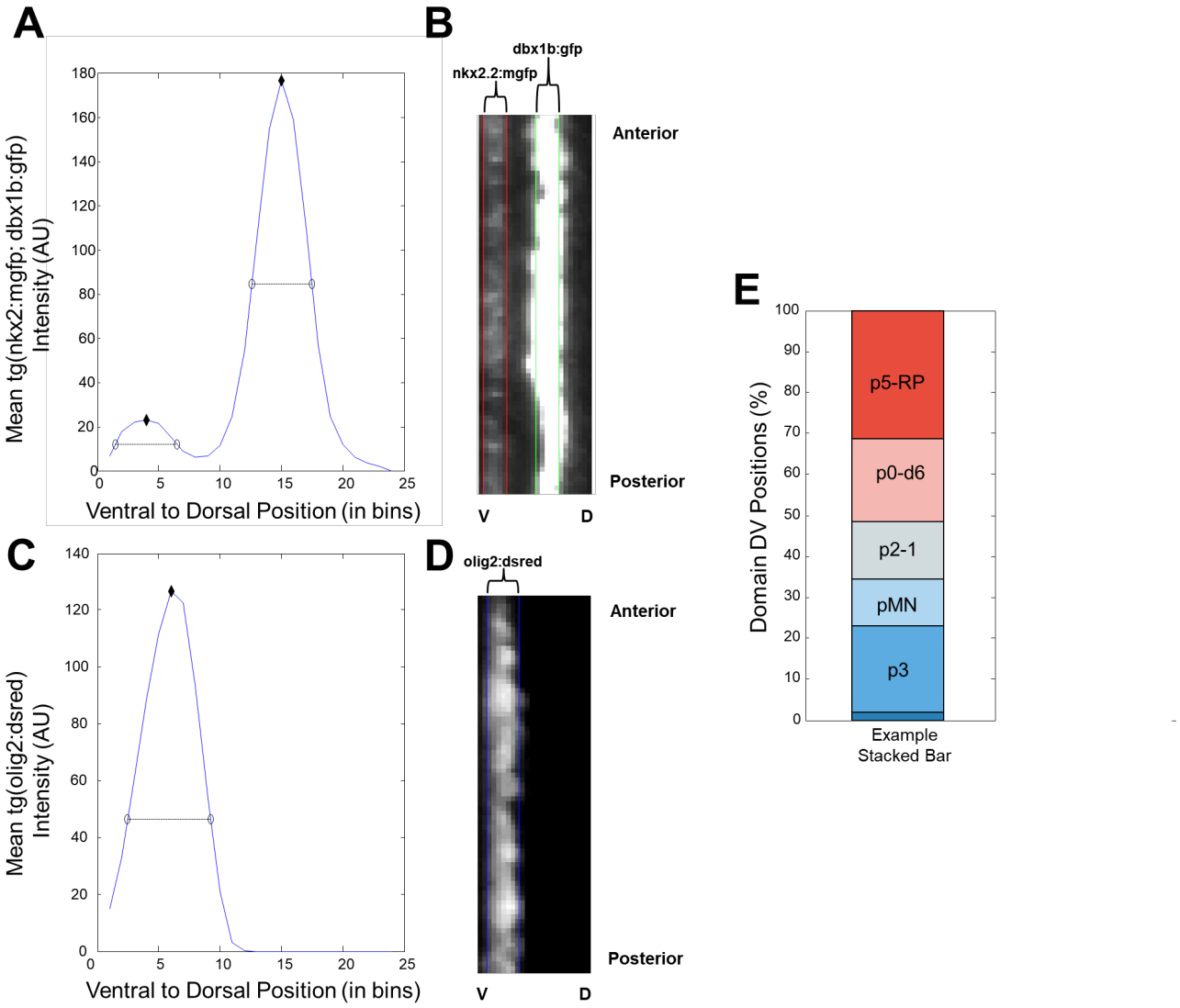

Figure S2- Progenitor domain width determination and bar plot generation.

(A) Averaged image intensity profiles from the green channel of both sides of a segmented neural tube from a *tg(dbx1b:GFP;olig2:dsred;nkx2.2a:memGFP)* embryo. Black diamonds represent peaks found by a peak finding algorithm, while open circles and lines show the calculated domain boundaries and width for this embryo based on the universally applied threshold in this dataset. Thresholds are determined by 50% of average peak intensity of the control population for each dataset. (B) Example domain determination of *nkx2.2a* and dbx1b+ cells. Red lines mark the predicted *nkx2.2a* domain, which correlates with the boundary of their fluorescence. Green lines mark the predicted width of the

863 *dbx1b* domain which correlates well with visible fluorescence of this domain. Some anterior-posterior
864 variability in domain size is observed. (C) Formatted as in part A, this plots the averages *olig2:dsred+*
865 intensity, peak, and determined width. (D) Example domain determination of *olig2+* cells. Blue lines
866 mark the predicted *olig2:dsred* domain, which correlates with the boundary of their fluorescence.
867 Thresholds are determined by 25% of average peak intensity of the control embryos in each dataset.
868 (E) Example stacked bar plot generated only from this embryo using calculated domain positions to
869 determine domain sizes.
870

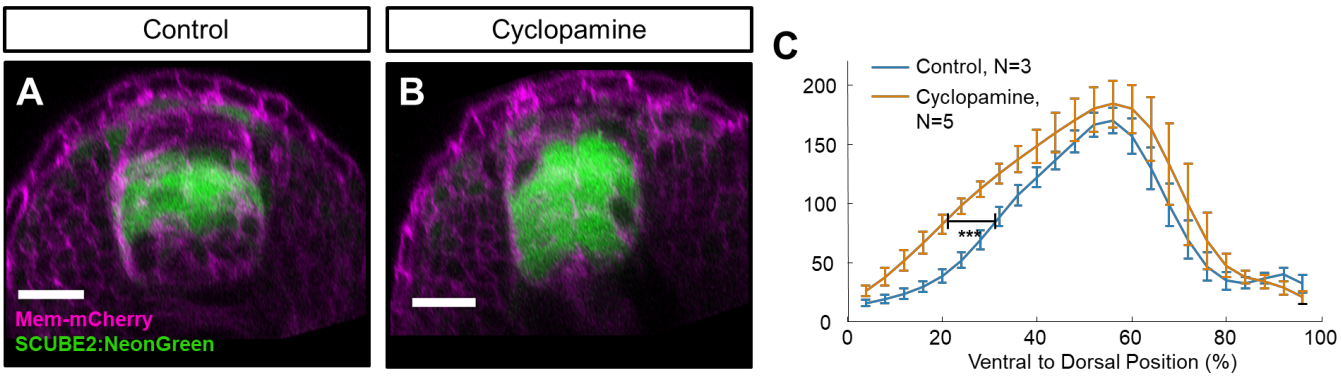

871

872

873 **Figure S3- Cyclopamine treatment of *tg(scube2:moxNG)* embryos.**

874 (A-C) Transverse view 22 hpf *tg(scube2:moxNG*; *mem:mCherry)* embryos treated with a DMSO control

875 (A) or 100µM Cyclopamine (B). (C) Quantification of mean reporter intensity of embryos as treated in A-

876 B. The black bar marks the position of 50% of control maximum intensity which was used for statistical

877 testing. These values were statistically significantly shifted ventrally in drug treated embryos relative to

878 control (unpaired t-test p= P=.0001145.).

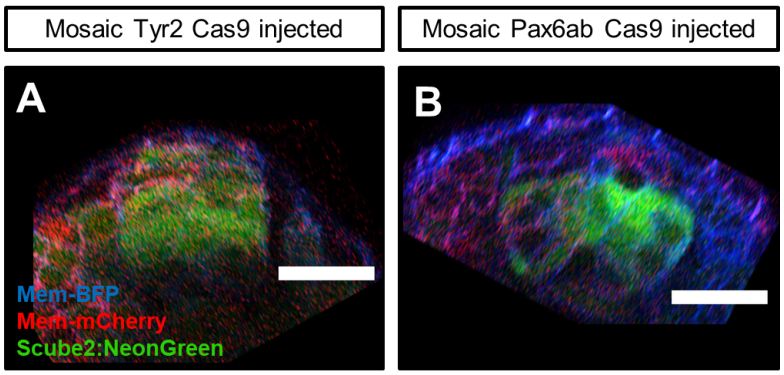

879

880

881 **Figure S4- Mosaic pax6a/b CRISPR mutants have lowered *scube2* expression.**

882 (A-B) *tg(scube2:moxNG)* embryos imaged at 18 hpf that were injected at the single cell stage with

883 *mem-mTagBFP2* mRNA and injected at the 8-16 cell stage with *mem-mCherry* mRNA, Cas9 protein,

884 and sgRNAs targeting either the tyrosinase pigment gene as a control (A) or *pax6a* and *b* (B).

885

886

887

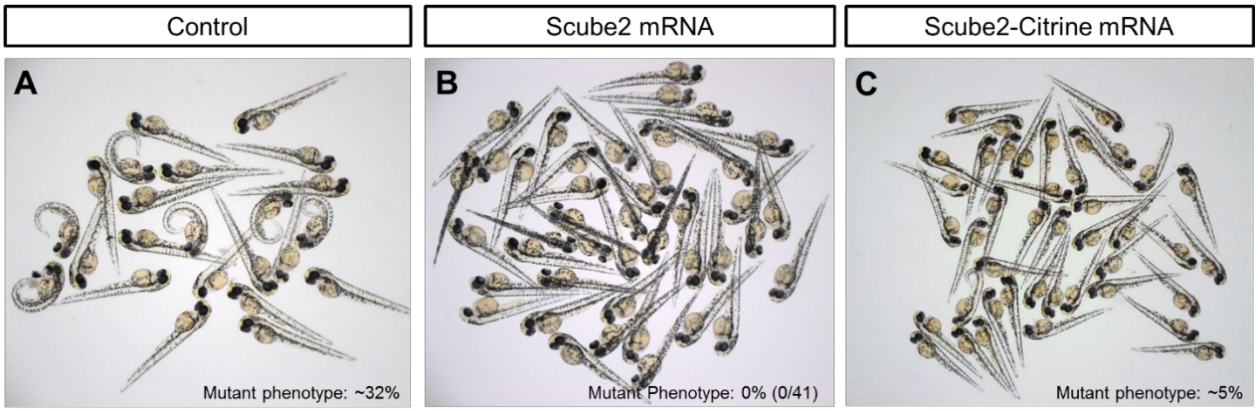

888

889 **Figure S5- Rescue of scube2 CRISPR mutants with *scube2* or *scube2-mCitrine* mRNA.**

890 (A) Results of a *scube2* mutant in-cross. The allele was generated by mutagenesis with CRISPR using

891 three guides targeting *scube2* coding sequence (B) Embryos rescued by the injection of *scube2* mRNA

892 co-injected with *mem-mCardinal* which were screened for being mem-mCardinal positive (Liu et al.,

893 2018). (C) Embryos rescued by the injection of *scube2-mCitrine* mRNA co-injected with *mem-*

894 *mCardinal* which were also screened for *mem-mCardinal* fluorescence.

895

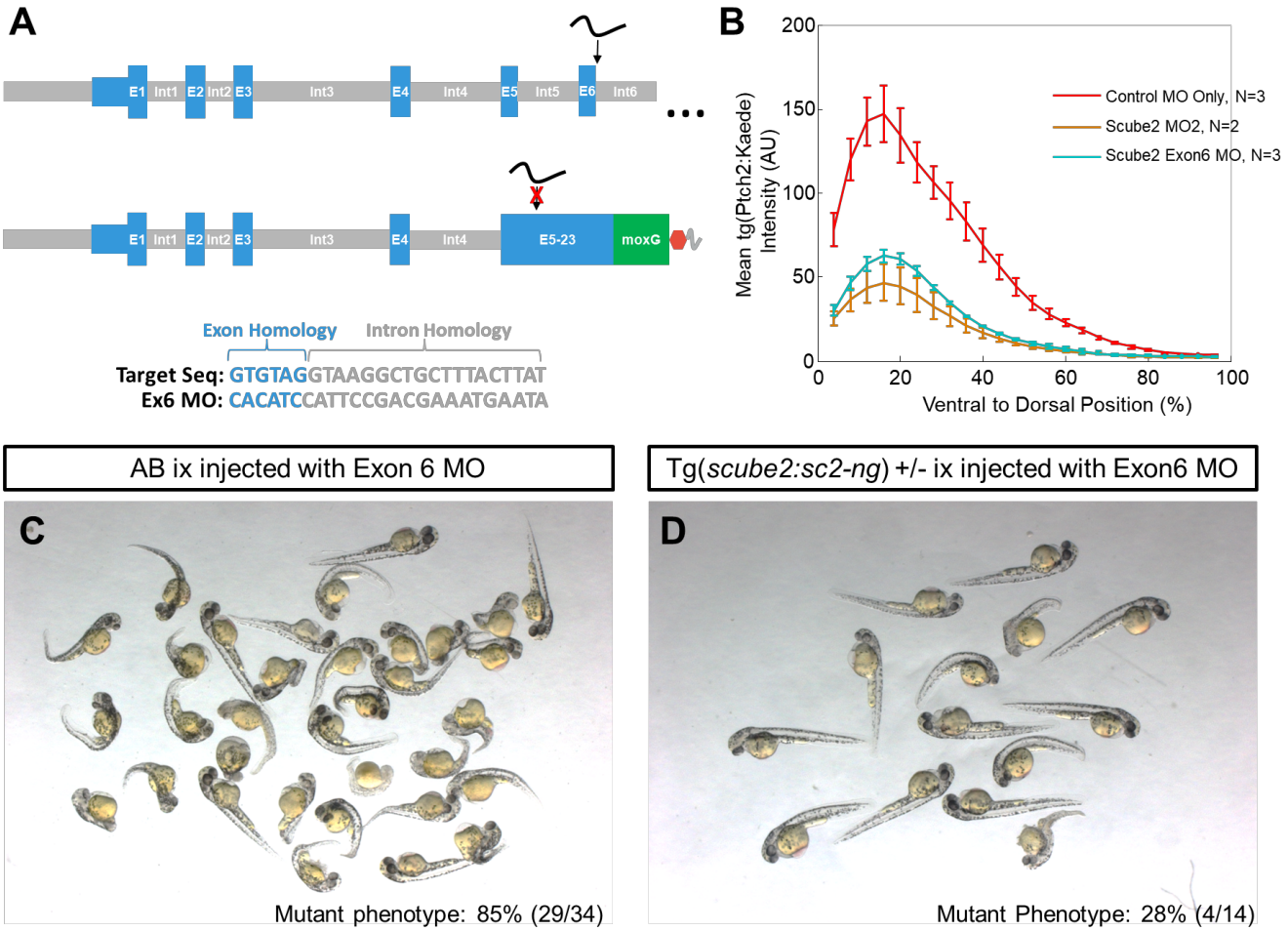

Figure S6- Rescue of morpholino knockdown by *tg(scube2:scube2-moxNeonGreen)* expression.

(A) Schematic of Scube2 Exon 6 targeting morpholino and expected resistance in the genome of *tg(scube2:scube2-moxNeonGreen)* embryos. Splice junction targeted by the Exon 6 morpholino is largely absent from the transgenic full length Scube2-mCitrine construct, allowing a test of rescue capacity. (B) *tg(ptch2:kaede)* response profiles of embryos injected wither with p53 morpholino only, the previously published Scube2 MO2 (Woods and Talbot, 2005), or Scube2 Exon 6 morpholino. (C) Overview photo of wildtype embryos injected with Scube2 Exon6 morpholino showing the tail curling indicative of Shh signaling phenotypes. (D) Overview photo of *tg(scube2:scube2-moxNeonGreen)* embryos injected with Scube2 Exon6 morpholino.

907

908

909 **Supplemental Movies:**

910 **Movie S1- *tg(scube2:moxNG; shh:mem-mCherry)* timelapse transverse view**

911 **Movie S2- *tg(scube2:moxNG; shh:mem-mCherry)* timelapse maximum intensity projection**

912 **dorsal view**

913 **Movie S3- Scube2-mCitrine FRAP imaging in a dome stage embryo**

914 **Movie S4- Sec-mCitrine FRAP imaging in a dome stage embryo**

915 **Movie S5- *tg(scube2:scube2-moxNG; shh:mem-mCherry)* timelapse transverse view**

916 **Movie S6- *tg(scube2:scube2-moxNG; shh:mem-mCherry)* timelapse maximum intensity**

917 **projection dorsal view**

918